Rock Mech Rock Engng (2008) 41: 797–834
DOI 10.1007/s00603-007-0160-9
Printed in The Netherlands

Rock Mechanics and Rock Engineering

A spatial estimation model for continuous rock mass characterization from the specific energy of a TBM

By

G. Exadaktylos[1], M. Stavropoulou[2], G. Xiroudakis[1], M. de Broissia[3], H. Schwarz[4]

[1] Department of Mineral Resources Engineering, Technical University of Crete, Chania, Greece
[2] Department of Dynamic, Tectonic and Applied Geology, Faculty of Geology and Geoenvironment, University of Athens, Greece
[3] Technical Department, Bouygues Travaux Publics, Saint-Quentin-en-Yvelines, France
[4] GISA Gestió d'Infraestructures, S. A., Barcelona, Spain

Received June 28 2007; Accepted November 14 2007; Published online 22 February 2008
© Springer-Verlag 2008

Summary

Basic principles of the theory of rock cutting with rolling disc cutters are used to appropriately reduce tunnel boring machine (TBM) logged data and compute the specific energy (SE) of rock cutting as a function of geometry of the cutterhead and operational parameters. A computational code written in Fortran 77 is used to perform *Kriging* predictions in a regular or irregular grid in 1D, 2D or 3D space based on sampled data referring to rock mass classification indices or TBM related parameters. This code is used here for three purposes, namely: (1) to filter raw data in order to establish a good correlation between SE and rock mass rating (RMR) (or tunnelling quality index Q) along the chainage of the tunnel, (2) to make prediction of RMR, Q or SE along the chainage of the tunnel from boreholes at the exploration phase and design stage of the tunnel, and (3) to make predictions of SE and RMR or Q ahead of the tunnel's face during excavation of the tunnel based on SE estimations during excavation. The above tools are the basic constituents of an algorithm to continuously update the geotechnical model of the rock mass based on logged TBM data. Several cases were considered to illustrate the proposed methodology, namely: (a) data from a system of twin tunnels in Hong Kong, (b) data from three tunnels excavated in Northern Italy, and (c) data from the section Singuerlin-Esglesias of the Metro L9 tunnel in Barcelona.

Keywords: Rock cutting, geostatistics, kriging, TBM, RMR, Q, specific energy

Correspondence: G. Exadaktylos, Department of Mineral Resources Engineering, Technical University of Crete, Chania, Greece
e-mail: exadakty@mred.tuc.gr

1. Introduction

A central problem of considerable practical interest in rock excavation engineering is how to predict spatial distribution of rock strength and possibly abrasivity over the tunnel length initially, using the conceptual 3D volume geological model, relevant geological interpretations (soft data) and limited number of samples obtained in the exploration phase (hard data), and subsequently to continuously upgrade this model by taking into account TBM registered data (hard data).

Herein, a first attempt is made to investigate whether initial rock mass geotechnical data sampled at the exploration phase may be used to predict the consumption of cutting energy by the TBM along the tunnel alignment or inversely if TBM logged data may be used for the mechanical characterization of rock masses either expressed by a rock mass classification index such as rock mass rating (RMR) or tunnelling quality index (Q) of the rock mass. This is beneficial for the design of tunnel support based upon rock mass classification systems and of the choice of TBM operational parameters for the best efficiency of the cutting process (i.e. minimization of specific cutting energy consumption) even before the commencement of excavation.

The algorithm presented below is as follows: in a first step relevant logged TBM parameters are used for the estimation of the Specific Energy (SE) of rock cutting; subsequently, considering SE to be a random function or regionalized variable the Kriging technique is applied to filter the raw TBM logged data and the in field mapping data of rock mass geotechnical properties for the tunnel under consideration. It is recalled that Kriging is an interpolation method for computing a minimum error variance linear estimate at a location where the true value is unknown (Journel and Huijbregts, 1978). Then, the simplest best-fitted empirical function that describes the dependency of the smoothed RMR on SE is found. The parameters of this function are calibrated by a best-fit procedure of TBM driving data when the latter passes through previously characterized rock mass sec-

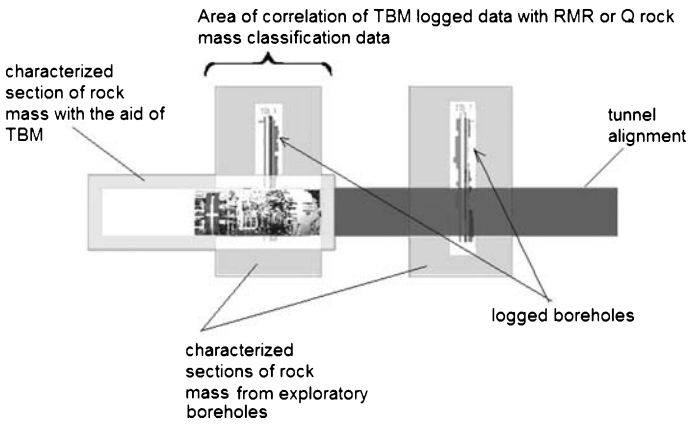

Fig. 1. Sketch of the concept of using TBM as a tool for geotechnical characterization of the rock mass between logged boreholes

tion by borehole logging and lab or in situ testing and mapping of tunnel walls and face, as illustrated in Fig. 1. Finally, the calibrated TBM model is used to improve the Kriging model of the heterogeneous rock mass by using not only the initial exploration data but also the TBM driving data as it is also shown in Fig. 1.

Recapitulating our objectives are the following:

- Knowing either RMR or Q rock mass classification indices to predict the consumption of the specific energy (SE) of the TBM along the alignment of the tunnel.
- Alternatively, by knowing SE to predict RMR (or Q) rock mass index and then to upgrade the ground model in front of the tunnel by combining with RMR (or Q) estimated from boreholes in front of the face of the tunnel.

Kriging of TBM parameters during excavation is performed by the KRIGSTAT code (Stavropoulou et al., 2007) further developed here for this purpose. A preliminary test of this code has been performed on TBM cutting data and RMR, as well as Q index measurements from: (a) a double tube tunnel in Hong-Kong, (b) three tunnels in northwestern Alps that have been thoroughly characterized and investigated previously by Sapigni et al. (2002) and Ribacchi and Lembo Fazio (2005), and (c) a tunnel bored in granodioritic rock mass for the construction of L9 Metro of Barcelona.

2. Basic design and operational TBM parameters

The operation of a TBM depends on many parameters that are related to the various operations performed by the machine and to the rock mass itself. The most important, however, are the parameters linked with the cutterhead because this is the part of the machine that is in direct contact with the rock mass through which the tunnel is passing, and more specifically the disc cutters (Fig. 2) that are transmitting the forces to the rock.

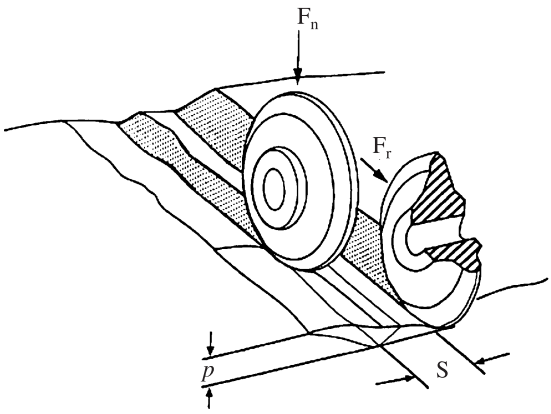

Fig. 2. Disc forces and geometry

The basic design and operational TBM parameters are given in the following list (where symbols L, F, and T enclosed in brackets denote the dimensions of length, force and time, respectively):

1. Cutterhead design: Cutterhead diameter, D [L], geometry of disc cutters (tip included angle (α) and curvature, thickness (w) or thickness for Constant Cross Section (CCS) cutters, diameter (2R) etc.), number (N), and position of discs (from this information about the mean spacing of neighbouring cuts, S [L], may be derived).
2. TBM operational mode (i.e. open, single or double shield, air compressed, slurry or Earth Pressure Balanced (EPB) etc.) and cutterhead shape (domed or flat). For example against the shield and during advance is acting the friction of the soil or rock mass.
3. Tunnel chainage (or ring number), C [L].
4. Cutterhead rotational speed, ω [1/T].
5. Orientation of tunnel (trend, plunge).
6. Linear velocity limit of the disc cutters, ν_{max} [L/T].
7. Power of the TBM motor, P [F L/T].
8. Total cutterhead thrust created by the push of the hydraulic jacks against the segments of the former ring, F [F].

The basic TBM parameters that are logged or calculated afterwards along the chainage are the following:

1. Cutterhead torque, T [F L].
2. Penetration per revolution, p [L].
3. Cutterhead (net) penetration rate, PR [L/T].
4. Disc cutter mean Normal (Thrust) Force, F_n [L].
5. Disc cutter mean Rolling Force, F_r [L].
6. Specific energy of cutting, SE [F L-2].
7. Cutterhead advance rate, AR [L/T].
8. Instantaneous or net cutting rate, ICR [L^3/T].
9. Disc cutter wear i.e. wear flat or cutter edge bluntness, W [L].
10. Life of disc cutters in [T], i.e. in units of time per cutter (that is also influenced by SiO_2 content of the rock or the content of other hard minerals).

The rock mass parameters that influence TBM performance include the following:

1. Rock porosity, microstructure and pre-existing microcracks
2. Rock hardness and abrasivity
3. Intact rock strength parameters (from appropriate failure criterion)
4. Rock mass joints (persistence, frequency, orientation, filling material, etc)
5. Ground water
6. Stress in rock.

Penetration rate (PR) is defined as the distance excavated divided by the operating time during a continuous excavation phase, while advance rate (AR) is the actual distance mined and supported divided by the total time and it includes downtimes for

TBM maintenance, machine breakdown, and tunnel failure (Barton, 2000). When using a TBM, it is necessary to choose a PR that matches the rate of debris removal and support installation. In conventional operations, the standard PR is decided beforehand and the other operations are timed to this rate.

Rolling forces are expressed as a function of the Cutting Coefficient denoted by the symbol CC and normal force according to the following equation

$$F_r = CC \cdot F_n \tag{1}$$

It may be shown that for uniform pressure distribution at the contact between the cutter and the rock the following relationship is valid (Rostami and Ozdemir, 1993)

$$CC = \tan\left(\frac{\varphi}{2}\right) \tag{2}$$

where φ is the angle of contact between the rock and the cutter, i.e.

$$\varphi = \cos^{-1}\left(\frac{R-p}{R}\right) \tag{3}$$

Roxborough and Phillips (1975) assuming that the resultant force passes through the centre of the disc cutter and is applied at the middle of the circular arc of contact derived an equivalent equation for CC

$$CC = \sqrt{\frac{p}{2R-p}} \tag{4}$$

The mean normal force acting on the disc cutters may be determined in a first approximation from the total measured thrust force F and the number of cutter disks N used by cutter machine as follows:

$$F_n = \frac{F}{N} \tag{5}$$

The torque T is the sum of the products of the radius of each disc cutter with rolling force, i.e.

$$T = \sum_{k=1}^{N} r_k F_r^k \tag{6}$$

where $r_k (k = 1, \ldots, N)$ are the radial distances of the disc cutters from the centre of the cutterhead and F_r^k denotes the rolling force of each kth disc cutter. The mean rolling force F_r may be estimated through the approximate formula

$$F_r \approx \frac{T}{0.3DN} \tag{7}$$

Fukui and Okubo (2006) proposed the following empirical relationships for the torque and thrust, respectively

$$T = c_2 UCSp^{3/2} \tag{8}$$

$$F = c_1 UCSp \tag{9}$$

where $c_1[L]$ and $c_2[L^{3/2}]$ are constants that depend on the number of disc cutters, diameter of cutters and diameter of the cutterhead. The second relation implies that the normal force increases linearly with penetration depth. This is in accordance with experimental results of various investigators (e.g. Gertsch et al., 2007). Dividing Eq. (8) and Eq. (9) by parts we obtain the result

$$\frac{T}{F} = \frac{c_2}{c_1}\sqrt{p} \tag{10}$$

The penetration depth per head revolution is given by

$$p = \frac{PR}{\omega} \tag{11}$$

The maximum cutterhead rotational speed $\omega_{\max}$ may be calculated from the formula

$$\omega_{\max} = \frac{\nu_{\max}}{\pi D} \tag{12}$$

that is to say, it is inversely proportional to TBM diameter (for example $\nu_{\max} = 150\,\mathrm{m/min}$ for 17-inch cutters).

The other TBM parameter of major importance is the Specific Energy (SE) of cutting which is defined as the energy consumed in removing a unit volume V of material (Kutter and Sanio, 1983)

$$SE = \frac{F_r \cdot \ell_T}{V} = \frac{F_r \cdot \ell_T}{p \cdot S \cdot \ell_T} = \frac{F_r}{p \cdot S} \tag{13}$$

in which ℓ_T is the total length traveled by the disc cutter, and S is the distance between neighbouring cuts (Fig. 2). It may be noticed that in the definition for SE only the rolling force is used because the rolling direction consumes almost all of the cutting energy whereas the energy expended in the normal direction is comparatively negligible. This is an immediate consequence of the fact that much greater amount of cutter travel takes place tangential to the face than normal to it, even though the normal force is much higher than the rolling. If SE is known then given the power of the TBM, the net cutting rate and finally the penetration rate can be found as follows:

$$\mathrm{ICR} = \eta\frac{P}{\mathrm{SE}} \Leftrightarrow \mathrm{PR} \cdot \frac{\pi D^2}{4} = \eta\frac{P}{\mathrm{SE}} \Leftrightarrow \mathrm{PR} = \frac{4\eta P}{\mathrm{SE}\pi D^2} \tag{14}$$

where η denotes the energy transfer ratio from the cutterhead to the rock mass.

The first hypothesis made in this work is the following:

Hypothesis #1: Herein we make the hypothesis that SE is independent from p, and depends solely on rock mass strength parameters (i.e. for a Mohr-Coulomb material from cohesion, tensile strength, internal friction and dilatancy angles) and perhaps on spacing of neighbouring cuts, S.

If this hypothesis is true then from formula (13) it may be inferred that the ratio F_r/p or the rolling force for constant p should increase linearly with increasing spacing of neighbouring cuts. This is in accordance with experimental evidence (i.e. Gertsch et al., 2007).

3. Analysis of geotechnical and TBM excavation data

In this section, five tunnelling case studies are considered in order to present the proposed algorithm. The first case refers to TBM excavation of a twin tunnel (double-tube) in Hong Kong with rock mass classification data from tunnel face mapping stored in a *relational database*. The next cases pertain to three tunnels excavated in Pieve, Varzo and Maen in northwestern Alps, Italy. The fifth case refers to a single tunnel bored in rock mass for the L9 Metro of Barcelona in which TBM logged data and rock core characterization from exploratory boreholes are available. The Kriging technique is used to filter or reduce properly the logged data referring to (a) RMR index as defined by Bieniawski (1973) that takes into account the effect of water but not the influence of tunnel orientation (in rock engineering practice it is called basic RMR but hereafter it is referred as RMR), (b) Q index as defined by Barton et al. (1974), as well as (c) the calculated SE of the TBM. It is noted here that in the considered case studies the cutters and the cutterhead were monitored only through total cutterhead thrust, torque, advance rate, etc. It would be a great improvement for operation of the machines to have the possibility to monitor representative cutters to register the instantaneous cutter loads. For mix-shield and EPB machines such instrumentation is vital to monitor real cutter loads, since the state of affairs of contact loads at the cutterhead of an EPB machine is very complex and difficult to estimate from the thrust cylinder pressure due to friction forces developed between the rock and the shield.

3.1 Hong Kong tunnel case study

The DB320 project was a part of the KCRC West Rail Project linking Mai Foo Station and Tsuen Wan West station in Hong Kong. The main features of the tunnel are displayed in Table 1.

Table 1. Main characteristics of the Mai Foo-Tsuen Wan West station tunnel system

Tunnel length	1840 m twin tunnel
Excavation diameter	8.75 m
Lining	
Ring length	1.8 m
Ring thickness	400 mm
Internal diameter	7.625 m
Distance between crosscuts	90 m

Table 2. Main geological profile along the Mai Foo-Tsuen Wan West station tunnel system

Section length	Rock types	Cover
200 m	hard granodiorite	up to 30 m
400 m	fair strength granite	up to 50 m
700 m	highly fractured and faulted granite	up to 50 m
200 m	mixed face (rock/soil)	15–25 m
300 m	soft soil made up of decomposed granite, alluvium and marine deposit	15 m

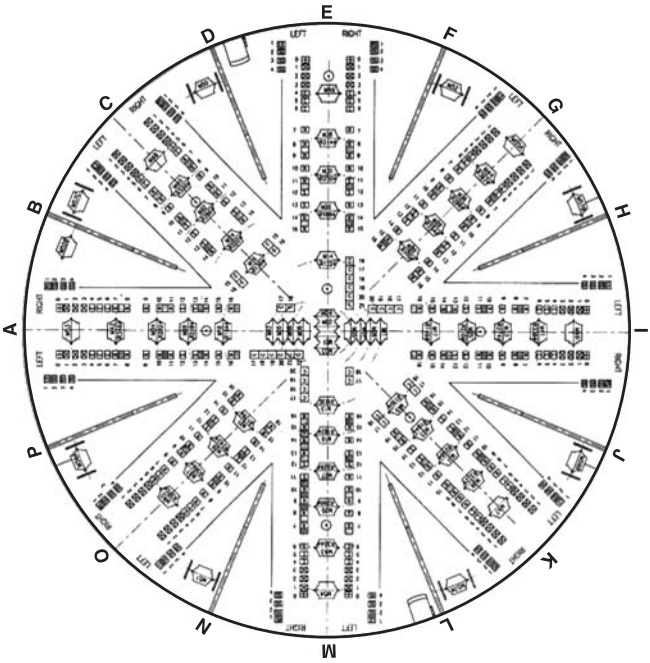

Fig. 3. Front view of the TBM cutterhead employed for the excavation of the twin tunnels in DB320 project

Table 3. Operating modes of the TBM along the tunnel

Chainage start	Chainage stop	Operating mode
0	600	open
600	800	air compressed
800	1260	open
1260	1300	air compressed
1300	1341	EPB
1341	1420	air compressed
1420	1820	EPB

Because of the mixed ground conditions that were encountered along the route of the excavation as is indicated in Table 2, the tunnel boring machine has been equipped to excavate both through soft ground conditions by operating in EPB mode, and through hard rock conditions by operating in Open Mode.

Table 3 shows the retained TBM operating mode as a function of the chainage of the tunnel whereas the cutterhead is shown in Fig. 3.

The rock mass classification data obtained from mapping of the tunnel face along the chainage of the tunnel were inserted in special Excel spreadsheets for the quick evaluation of the RMR and Q parameters. It is noted here that both a minimum and a maximum value of the respective rock mass classification index were calculated based on the assessed range of variation of one or more parameters affecting their values (i.e. maximum and minimum values of RQD, joint spacing or ground water index, etc.).

Ring_number	Chainage	Thrust	Torque	ch_speed	ch_power	tbm_speed	penetration	mode
	m	F (tn)	kN m	rpm	%	mm/min	mm/rev	
1	11.1	1036	2243	1.54		4	2.60	N/A
2	12.9	1692	2796	1.54		16	10.39	Open
3	14.7	1170	2300	1.54	15	12	7.79	Open
4	16.5	1200	2700	1.54	17	9	5.84	Open
5	18.3	1560	2900	1.88	23	20	10.64	Open
6	20.1	1550	2680	1.88	24	22.5	11.97	Open
7	21.9	1780	3200	1.88	26	17	9.04	Open
8	23.7	1623	3093	1.88	26	18	9.57	Open
9	25.5	1748	4146	1.86	38	25	13.44	Open
10	27.3	1554	2790	1.88	23	13.5	7.18	Open
11	29.1	1570	2816	1.88		14	7.45	Open
12	30.9	1734	2581.5	2.12		17	8.02	Open
13	32.7	1640	2343	2.12	23	15	7.08	Open
14	34.5	1470	2624	2.12	23	16	7.55	Open
15	36.3	1504	3455	2.12	23	16	7.55	Open
16	38.1	1460	2400	2.12	24	18	8.49	Open
17	39.9	1480	3000	2.2	24	22	10.00	Open
18	41.7	1597	2927	2.2	24	18	8.18	Open
19	43.5	1571.5	2273.5	2.78	25	18	6.47	Open
20	45.3	1250	2586	2.78	25	38	13.67	Open

(a)

Chainage	MIN RMR basic	MAX RMR basic	MIN RMR89	MAX RMR89		Rock type
13.05	58	71	63	76	13.05 (0)	GRANIODIORITE
14.85	67	80	72	85	14.85 (3)	GRANIODIORITE
16.81	66	78	66	78	16.81 (3)	GRANIODIORITE
22	58	68	63	73	22 (-)	GRANIODIORITE
23.8	66	78	66	78	23.8 (8)	GRANIODIORITE
29.76	66	78	66	78	29.76 (11)	GRANIODIORITE
33.79	62	86	62	86	33.79 (-)	GRANIODIORITE
40.08	68	85	68	85	40.08 (17)	GRANODIORITE
43.6	53	76	61	76	43.6 (-)	GRANODIORITE
45.3	51	61	59	69	45.3 (-)	GRANODIORITE
52.6	58	67	63	72	52.6 (24)	GRANODIORITE
54.6	51	64	56	69	52.6 (24)	GRANODIORITE
65.2	58	66	63	71	65.2 (30)	GRANODIORITE
68.28	64	79	69	79	68.28 (-)	GRANODIORITE
77.7	82	93	82	93	77.7 (37)	GRANODIORITE
84.9	63	80	63	80	84.9 (41)	GRANODIORITE
92.2	83	94	83	94	92.2 (45)	GRANODIORITE
95.7	63	80	68	80	95.7 (-)	GRANODIORITE
99.3	56	64	61	69	99.3 (49)	GRANODIORITE(60%)-GRANITE (40%)
108.36	56	64	61	69	108.36 (54)	GRANODIORITE(60%)-GRANITE (40%)

(b)

Chainage [m]	RQD-min	RQD-max	Jn	Jw	Jr	Ja	Qmin	Qmax
13.05	75	90	3	0.9	2	6	7.5	9.0
14.85	75	90	3	0.9	1.5	6	5.6	6.8
16.81	90	100	3	1	2	6	10.0	11.1
22	90	100	3	1	2.5	6	12.5	13.9
22	90	100	3	1	2.5	6	12.5	13.9
22	90	100	3	1	2.5	6	12.5	13.9
23.8	90	100	3	1	2	6	10.0	11.1
29.76	90	100	3	1	2	6	10.0	11.1
33.79	90	100	3	1	2.5	1	75.0	83.3
33.79	90	100	3	1	2.5	10	7.5	8.3
33.79	90	100	3	1	2.5	0.75	100.0	111.1
40.08	90	100	3	1	2.5	6	12.5	13.9
43.6	90	100	3	1	2.5	1	75.0	83.3
43.6	90	100	3	1	2.5	10	7.5	8.3
45.3	75	90	3	0.6	2.5	6	6.3	7.5
52.6	75	90	6	0.9	2	0.75	30.0	36.0
52.6	75	90	6	0.9	2	0.75	30.0	36.0
54.6	75	90	6	0.9	2	10	2.3	2.7
54.6	75	90	6	0.9	2	10	2.3	2.7
54.6	75	90	6	0.9	2	6	3.8	4.5

(c)

Fig. 4. Excel worksheets referring to (a) TBM logged parameters at 696 stations along the tunnel (b) RMR estimations at 151 stations along the tunnel, and (c) Q rock mass classification index estimations at 281 stations along the chainage of tube (1) where J_n is the joint set number, J_r is the joint roughness number, J_a is the joint alteration number, J_w is the joint water reduction factor

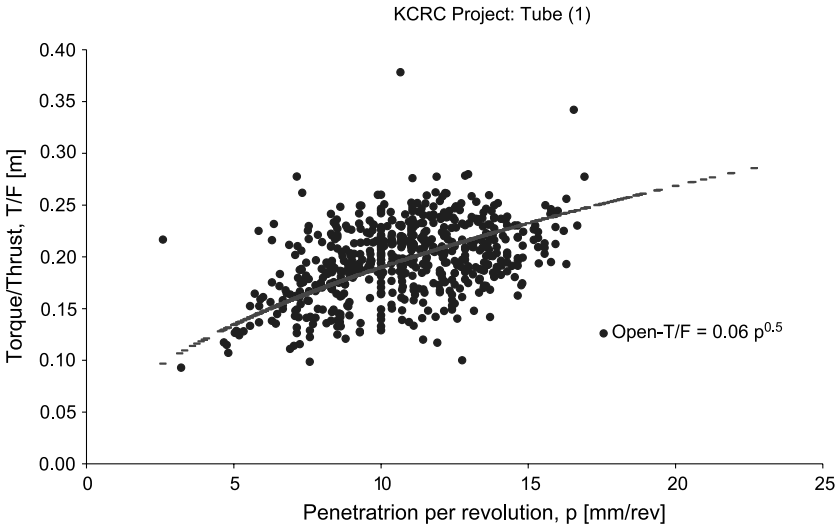

Fig. 5. Relationship between torque/thrust ratio and penetration per revolution derived by best-fitting a power curve

Subsequently as illustrated in Fig. 4a–c, three separate worksheets were created containing TBM parameters, RMR and Q evaluations, respectively, for the geostatistical analysis.

Since for this case study both thrust and torque data were available, the formula proposed by Fukui and Okubo (2006) relating the torque/thrust ratio with the penetration depth (or cutting depth) per revolution is checked in a first place. Figure 5 presents the logged data from tube #1 and the best fit power law which is in accordance with that proposed by the previously mentioned authors, i.e.

$$\frac{T}{F} = 0.06\sqrt{p}, \quad [T/F] = \text{m}, \ [p] = \text{mm} \tag{15}$$

Subsequently, composited (i.e. smoothed) data of rock mass indices or SE of TBM are used with the purpose to filter the respective raw data in order to establish a good correlation between SE and Rock Mass Rating (RMR) (or tunnelling quality index Q) along the chainage of the tunnel. This composition of data introduces some smoothing that would be better avoided for the prediction of a parameter at hand (i.e. SE, Q or RMR) from measurements using the Kriging technique; however, as it was already mentioned in this work we want primarily to delineate the better phenomenological relationship among rock quality and specific energy consumption.

In a first step the subroutine RANDCOMP of the geostatistical analysis code KRIGSTAT (see Appendix A) was used for the composition of raw RMR data in order to refer to the same length of tunnel (that is called ''support'' in Geostatistics). A search radius 20 m was applied over a grid of 9 m intervals, which is also the mean distance between measurements. The mean value of the variable of interest formed by its sampled values inside this radius was computed and assigned to the grid-point at the centre. The raw and composited max RMR data as well as the raw min RMR data

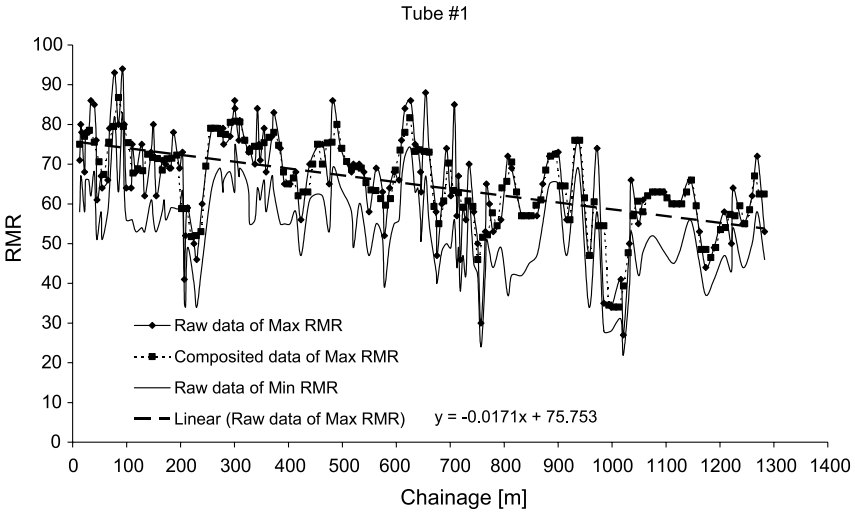

Fig. 6. Comparison of raw and composited max RMR along tube #1

along the chainage indicating the range of variability of rock mass quality are shown in Fig. 6. Also, the frequency histogram of RMR values is illustrated in Fig. 7a.

Hypothesis #2: The second hypothesis we make in this work is that RMR, Q and SE are spatial attributes that can be modelled as random functions. It should be noticed that field measured quantities cannot be random functions; they only can be modelled as random functions. It may be also recalled here that a random field or stochastic process denoted as $X(S)$, wherein S denotes the position vector in space, is the rule to correspond to every outcome ζ of an experiment a function $\underset{\sim}{X}(S, \zeta)$.

Hypothesis #3: After the removal of the possible trend of data, the mean of RMR, Q or SE random functions in the neighbourhood of the estimation is constant but unspecified and the two-point mean square difference depends only on the distance between two locations. This is the so-called "intrinsic isotropic model" of Geostatistics (Kitanidis, 1997).

The consequent step is the construction of the experimental semivariogram of RMR values via the subroutine SEMIVAR (e.g. Appendix A). The semivariogram is a quantitative descriptive statistic characterizing the spatial continuity of a data set. It is a random function whose values that are described in statistical sense depend on spatial position, is commonly used as a tool to quantitatively describe the spatial property of the domain (assuming of course that such spatial dependence exists). It is a measure of the dissimilarity between properties (the covariance between two values) that are located a distance h apart. The estimate of variance is repeated for many values of h to represent the spatial correlation of the property being analyzed. This similarity measure is denoted by the symbol $\gamma(h)$ and it is plotted on an x–y plot with the x-axis being the distance h, and $\gamma(h)$ on the y-axis. The experimental semivariogram is defined as half of the average squared difference between two attribute

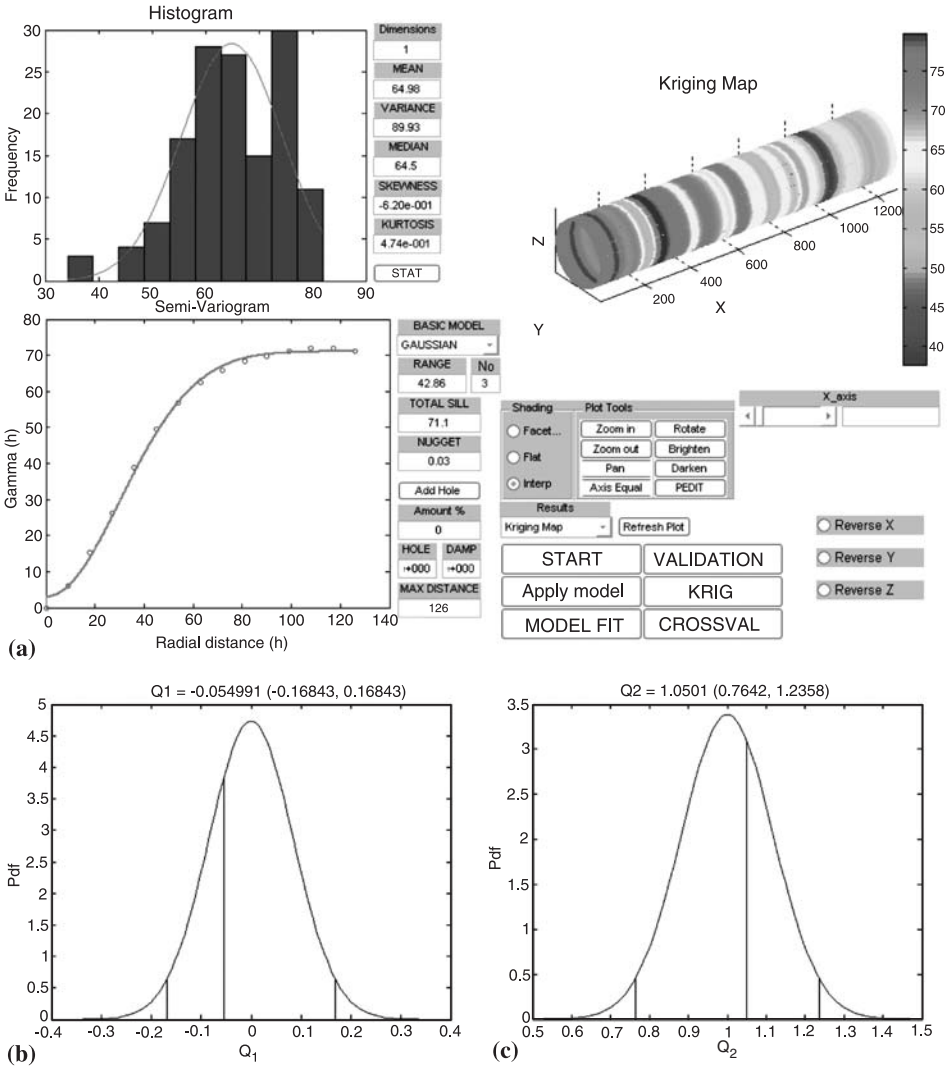

Fig. 7. Presentation of KRIGSTAT results: (a) Frequency histogram of composited max RMR values and experimental semivariogram with best-fitted Gaussian semivariogram model (range = 75 m, sill = 71.1 and nugget = 3), as well as visual representation of predicted RMR along tube #1; validation of Kriging model with (b) Q_1 test, and (c) Q_2 statistical test

values approximately separated by vector h_i which is also called lag. Here the computation of the semivariogram is based on the *Mean Ergodic Hypothesis* (*Hypothesis #4*) (Papoulis, 1984) that permits the substitution of the stochastic mean value with the mean value of all the couples of measurement points that are approximately at distance h apart. This in turn implies that the process is regular or statistically homogeneous to ensure that, from a unique realization of the process, there is a representation of all possible values that the process can attain.

After examination of several semivariogram models by virtue of subroutine QVAL (Appendix A), the Gaussian model was finally selected since this was eventually found to give the best Q-statistic validation values. This model that is shown graphically in Fig. 7b is expressed by the equation

$$\gamma = C_0 + \sigma^2\left[1 - \exp\left(-\left\{\frac{h}{\ell}\right\}^2\right)\right] \tag{16}$$

where h [L] denotes the lag, the parameter ℓ [L] denotes the range of influence that is equal to $7\ell/4$, σ^2 is the sill and C_0 is the nugget effect. Nugget represents unresolved, sub-grid scale variation or measurement error and is seen on the semivariogram as the intercept of the semivariogram. The range is the scalar that controls the degree of correlation between data points, usually represented as a distance. Sill is the value of the semivariance as the lag goes to infinity, it is equal to the total variance of the data set. Also, in order to attain a better fit, the used semivariogram points were limited to the first 120 m. The next step pertains to the Kriging estimations at any location between the sampled positions. It is obvious from Fig. 6 that a linear global trend existed to the data. Therefore, Universal Kriging was employed as the most appropriate interpolation technique. In this technique the prediction process begins with transformation of sample values by subtracting the trend portion of the value. Predicting the spatial variation of the residual portion follows the ordinary Kriging steps, and once this is complete we add back the trend portion.

The validation of the assumed Kriging model that is based on the semivariogram model given by (16) and the associated Kriging parameters was performed in this case by virtue of Q_1 and Q_2 statistical tests (Kitanidis, 1997). Q_1 and Q_2 cross validations are used to check the statistical distribution of the residuals between the observed data and Kriged values at the original observation locations by using the same Kriging parameters and semivariogram model parameters. To perform Q_1 and Q_2 cross validations, a normalized residual array $\{\varepsilon_k\}, k = 1, \ldots, n$ needs to be constructed. It is recalled here that residuals are the differences between observations and model predictions. That is, Q_1 checks the statistics of the mean of the residual ε_k and approximately follows the normal distribution, while Q_2 checks the statistics of the variance of ε_k, also $Q_2(n-1)$ approximately follows the chi-square distribution with parameter $n-1$. Both tests for the RMR are shown graphically in Fig. 7b and c, respectively. The acceptable region defined in the program is delimited by the two vertical lines that correspond to the 0.025 and 0.975‰ as is illustrated in Fig. 7b and c. As it may be seen from these figures the Kriging model passes these specific validation tests successfully.

The maximum values of the tunnelling quality index Q estimated at 281 stations along tube #1 are next analyzed by virtue of the Kriging technique. The maximum Q index was considered subsequently (as also in the case of RMR) in order on one hand to implicitly take into account the "size effect" exhibited by the rock strength that means that the strength of the rock at the scale of the cutting with the disc cutters of the TBM (few centimetres) is larger than that at the larger scale of the tunnel (few meters), and on the other hand to consider the worst case in terms of specific energy consumption of the TBM. A spheroidal searching mask with 10 m radius sliding on a

9 m grid intervals was applied to the original data using again the subroutine RANDCOMP. Based on the Kolmogorov-Smirnov normality test (via the subroutine KST in Appendix A) it was inferred that Q data do not follow the normal (Gaussian) distribution; instead it seems that are fitted well with the lognormal distribution.

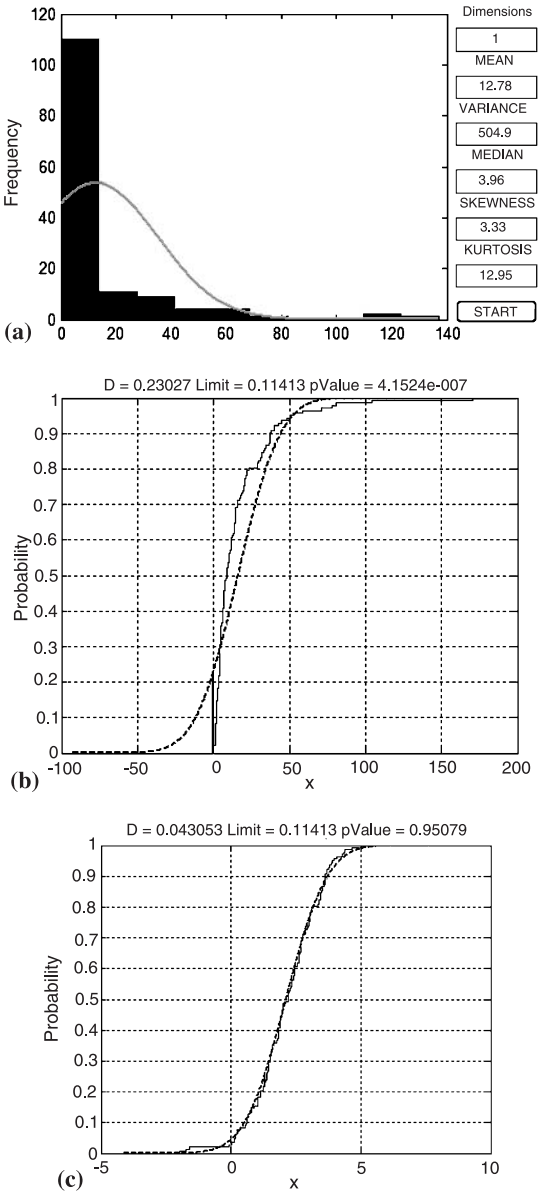

Fig. 8. (a) Frequency histogram of composited max Q data; (b) probability plot of composited data; and (c) probability plot of log-transformed data

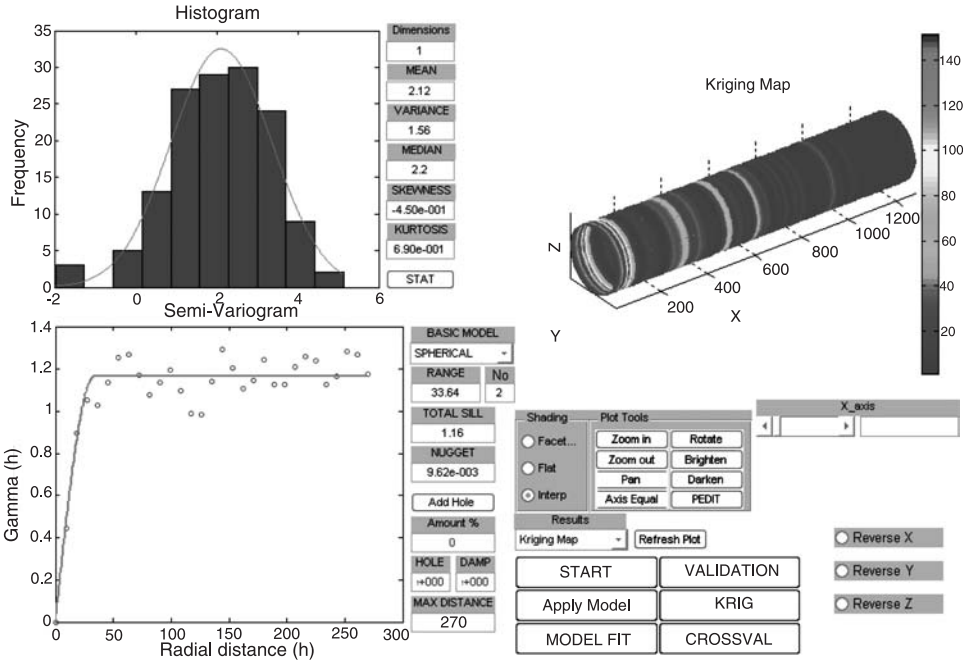

Fig. 9. Histogram of composited log-transformed max Q values, experimental semivariogram and best-fitted spherical function (range = 33.64 m), as well as visual representation of predicted max Q values along tube #1

For that reason a logarithmic transformation was applied to the original sampled data by virtue of the subroutine TRANSVAL. Figure 8a–c illustrate the above referenced steps of preliminary classical statistical analysis.

Subsequently the experimental semivariogram of transformed Q_{max} data was fitted by a spherical model as it is shown in the following Fig. 9. This model is described by the following equation

$$\gamma(h) = \begin{cases} C_0 + \sigma^2 \left[\frac{3}{2}\frac{h}{\ell} - \frac{1}{2}\left(\frac{h}{\ell}\right)^3 \right], & \text{for } h \leqslant \sigma^2 \\ C_0 + \sigma^2, & \text{for } h > \sigma^2 \end{cases} \tag{17}$$

As it is shown in Fig. 10a and b the validation with use of both Q_1 and Q_2 statistical tests was successful so the theoretical semivariogram model given by Eq. (17) is acceptable for the Kriging interpolation.

The final predictions were found after the following backward transformation that is performed in the TRANSVAL subroutine

$$Q^* = e^{Q^l} \tag{18}$$

where Q^* denotes the predictions corresponding to the original data following the lognormal distribution and Q^l the Kriging predictions corresponding to the log-transformed data that obey the normal distribution. After the prediction of the distribution

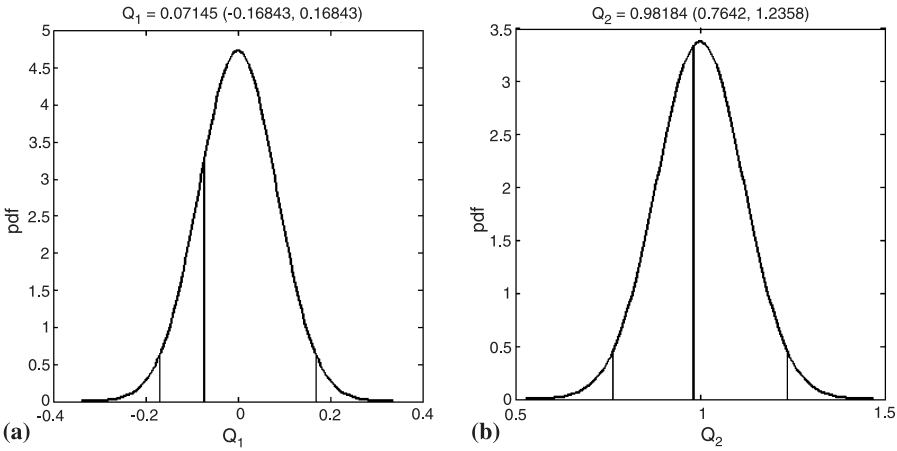

Fig. 10. (a) Q_1 statistic and (b) Q_2 statistic

of Q index at the same locations where also RMR has been estimated, the best-fitted logarithmic relation linking these two indices was found as follows

$$\mathrm{RMR} = 6.1 \ln Q + 52.28 \tag{19}$$

It should be noticed that Q and RMR values were estimated with Kriging at points along the tunnel with maximum distance from the measurements in neighboring points always less of 9 m which is much lower than the range of influence of both RMR and Q.

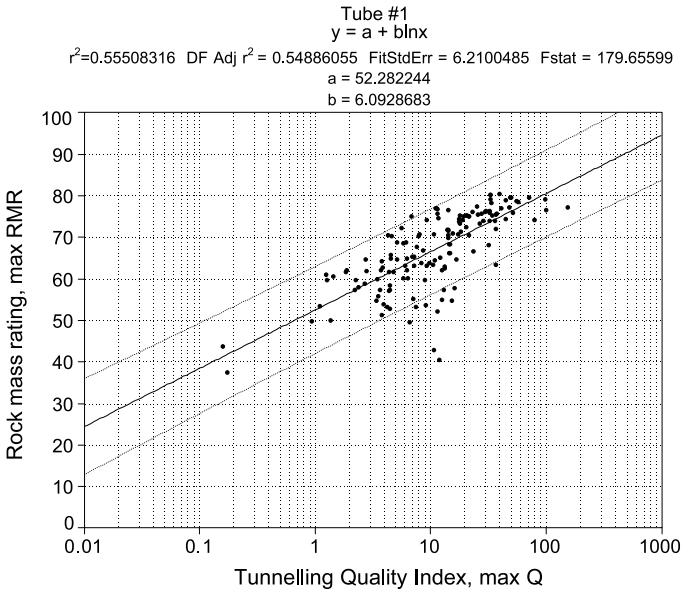

Fig. 11. Dependence of BRMR on Q found in tube #1 with best-fit logarithmic relation and 90% prediction limits

Therefore, the Kriging errors are compatible for both indices (i.e. lower than 5% of the sill) and their correlation with (19) is valid. Figure 11 displays graphically the above relationship together with the 90% upper and lower prediction limits (i.e. 90% probability that the points fall inside this envelope). Having demonstrated that there is a relation between RMR and Q, we proceed in the sequel with the former index.

In a further step of the proposed methodology, the spatial analysis of specific energy of TBM cutting is performed. SE was estimated from the original sample of size 696 by computing first the rolling force from the registered torque

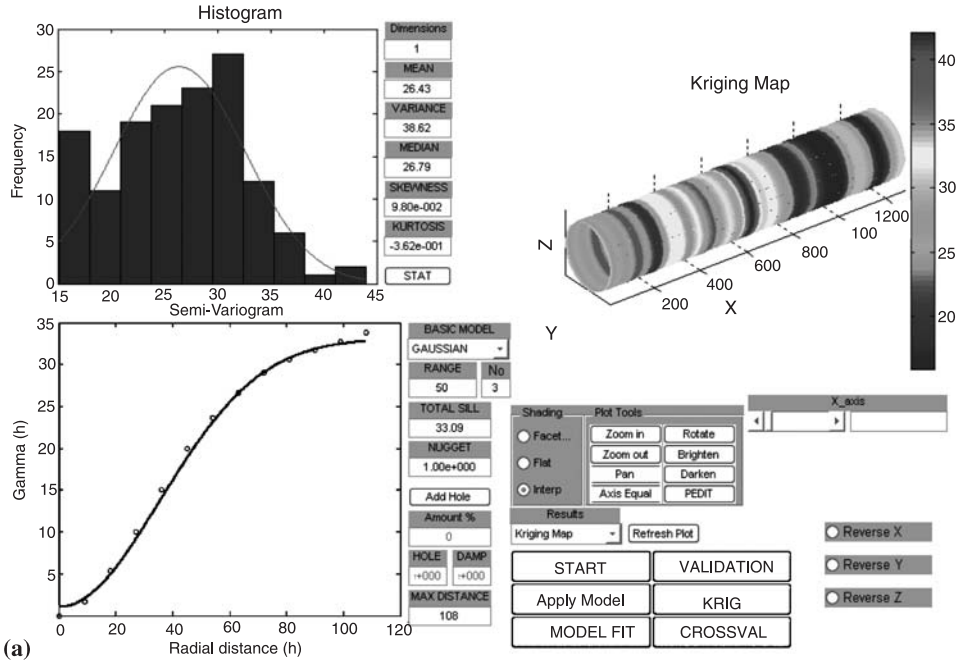

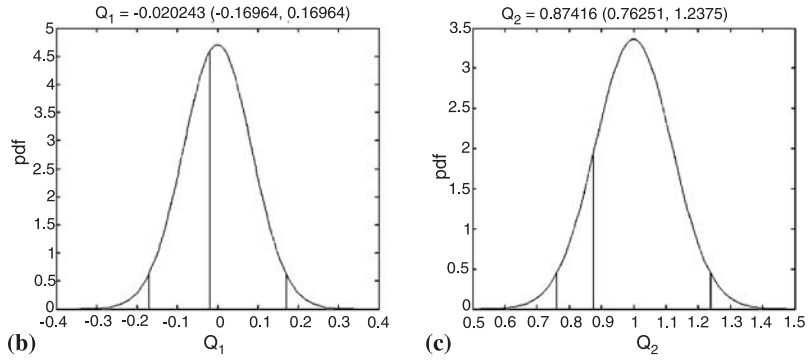

Fig. 12. (a) Frequency histogram of composited SE values, experimental and fitted Gaussian semivariograms for SE (range = 87.5 m, sill = 33.09 and nugget = 1); Validation of Kriging results with (b) Q_1 test and (c) Q_2 test

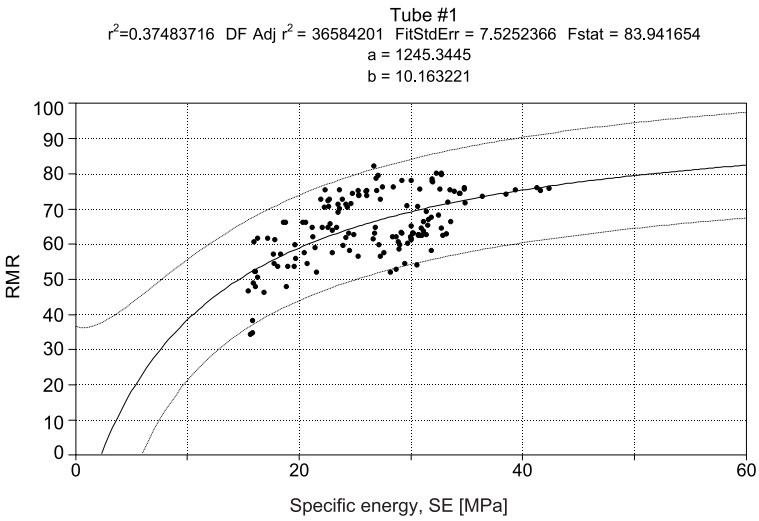

Fig. 13. Dependence of RMR on SE with 95% prediction intervals

via Eq. (7), then the penetration depth per revolution via formula (11) and finally estimating SE from relation (13) with an estimated mean spacing between neighboring cuts $S = 0.075$ m. For that case also a same filter (i.e. 20 m search radius on a 9 m grid) was applied for data compositing. The frequency histogram that resembles the normal distribution is shown in Fig. 12a. The experimental semivariogram of SE together with the best fitted Gaussian model are shown also in Fig. 12a, whereas the Q_1, Q_2 validation tests results are graphically presented in Fig. 12b and c, respectively.

In a subsequent stage, the RMR and SE predictions at each common Kriging point along the tunnel are placed in the same diagram and the simplest possible mathematical function that best fitted the data was found. As it is illustrated in Fig. 13 smoothed SE and RMR data along the chainage of the tube #1 were found to exhibit the following simple hyperbolic relationship

$$\begin{gathered} \mathrm{RMR}_{\max} = 100 - \frac{a}{SE + b}, \quad [\mathrm{SE}] = \mathrm{MPa} \\ a = 1253\,\mathrm{MPa} \text{ and } b = 10\,\mathrm{MPa} \end{gathered} \tag{20}$$

where a and b are free parameters depending on the machine and excavated rock mass formations. It may be noted that the above phenomenological relation gives always $\mathrm{RMR} = 100$ as $\mathrm{SE} \to \infty$.

By employing the above hyperbolic relation and original estimated SE data along the sampled tunnel stations the predicted RMR values are compared with actual sampled RMR values in a back-analysis procedure (Fig. 14). From this figure it may be seen that SE estimations and predictions are in acceptable agreement.

Based on the phenomenological relation (20) of max RMR with SE derived from Tube #1 database, as well as the logged SE data along Tube (2) at 97 stations, the max RMR along Tube #2 was predicted and plotted in Fig. 15. By recalling that the max

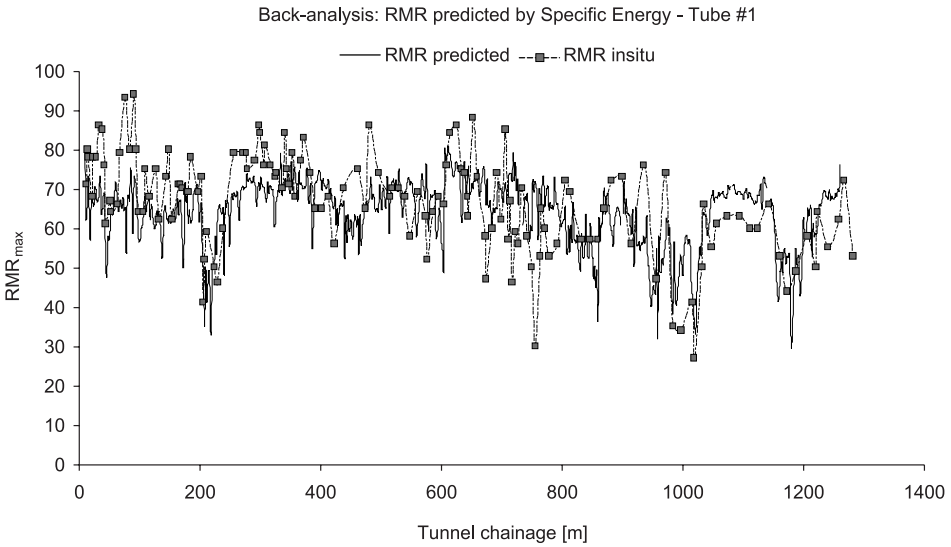

Fig. 14. Raw and predicted RMR data by using the hyperbolic formula

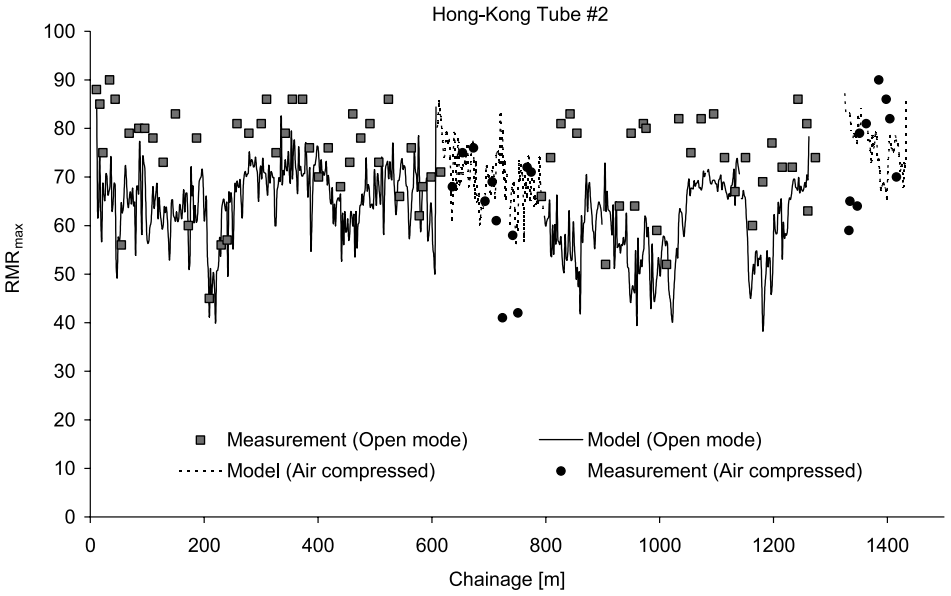

Fig. 15. Logged and predicted max RMR index along tube #2 by using the hyperbolic formula and SE logs derived from analysis of data along tube #1

RMR values were estimated independently from the relational database of tunnel mapping logs of geotechnical data, it may be inferred that the empirical formula (20) predicts RMR values with acceptable accuracy.

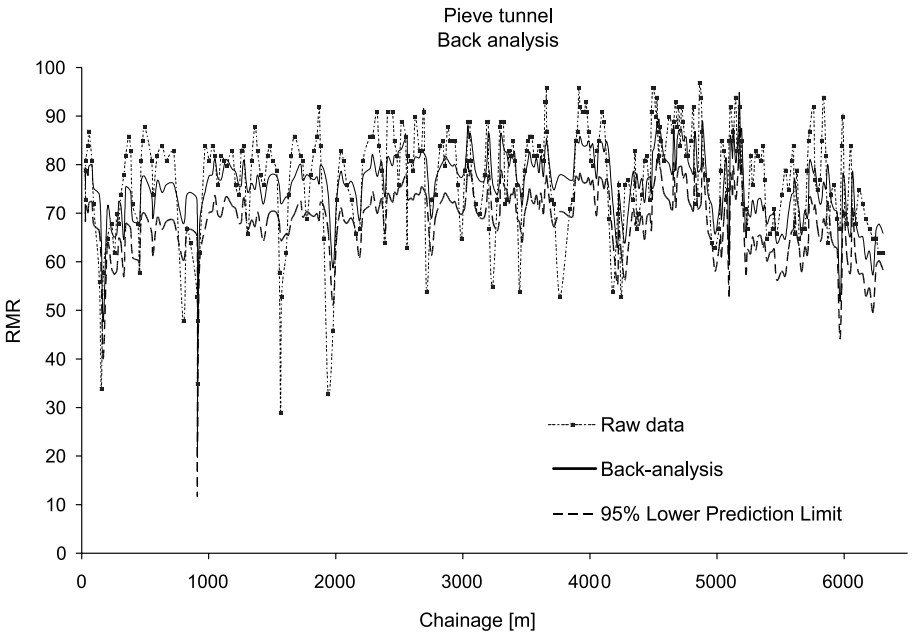

(a)

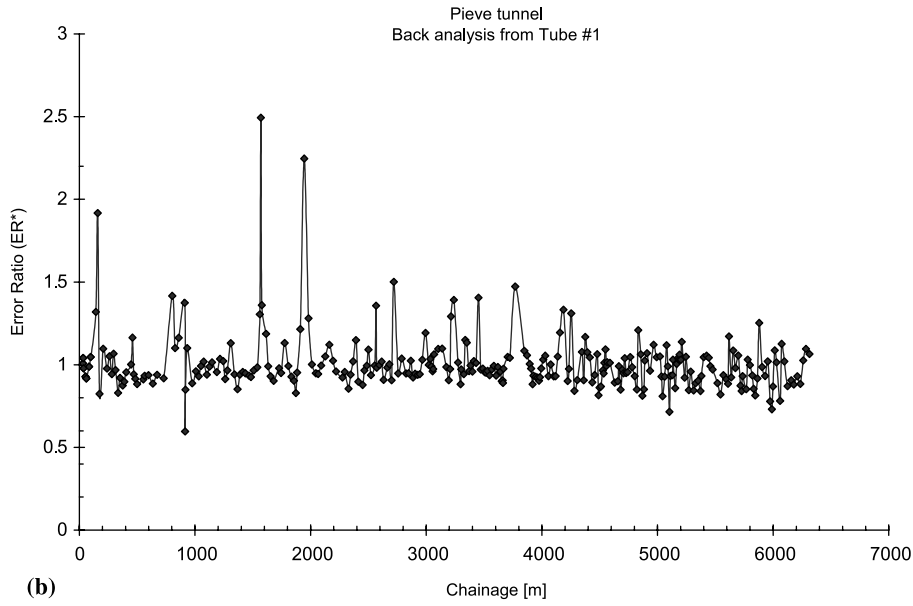

(b)

Fig. 16. (a Comparison of the estimated in field and predicted RMR together with the lower 95% prediction limit along the chainage of the Pieve tunnel by using calibrated hyperbolic relation from the first 400 m of the tunnel; (b) plot of error ratio (= prediction/measurement)

3.2 Pieve, Varzo and Maen tunnels

The next step for the validation of the formula (20) relating RMR with SE, is to estimate the calibration hyperbolic model parameters a, b by requiring the minimization of the error-squared of the predictions for the RMR at the initial stage tunnel excavation. This was done for the case of Pieve tunnel for which data were available (Sapigni et al., 2002). For this case the raw data for RMR and SE referring to the first 400 m were used for the estimation of constant parameters a, b in (20). This minimization procedure lead to the estimation of

$$a = 1746.6\,\text{MPa} \quad \text{and} \quad b = 0.71\,\text{MPa} \tag{21}$$

that may be compared with the parameters found from the previous case study (i.e. a = 1253 MPa and b = 10 MPa). Through the regression analysis the upper and lower bounds of these parameters corresponding to the 95% prediction limits have been found. The comparison of the above relation (21) based on the logged SE of the TBM with measured RMR along Pieve tunnel at 300 stations is shown in Fig. 16a, b. It is worth noticing here that if the complete set of raw (SE, RMR) data is considered for the calibration of model parameters then the estimated values of a, b would be

$$a = 1806\,\text{MPa} \quad \text{and} \quad b = 5.24\,\text{MPa} \tag{22}$$

which are not much different from the above set of values indicated in (21).

The next case is a hydraulic tunnel 6.6 km long, built for the Varzo pumped storage plant (owned by ENEL) which was completed in 2001, presented by Ribacchi and Lembo Fazio (2005), as well as in the paper by Sapigni et al. (2002). The tunnel is located in Piedmont near the Simplon pass (Western Alps) and runs along the Southern slope of the Diveria valley in East–West direction (E5° N–E15° N). The

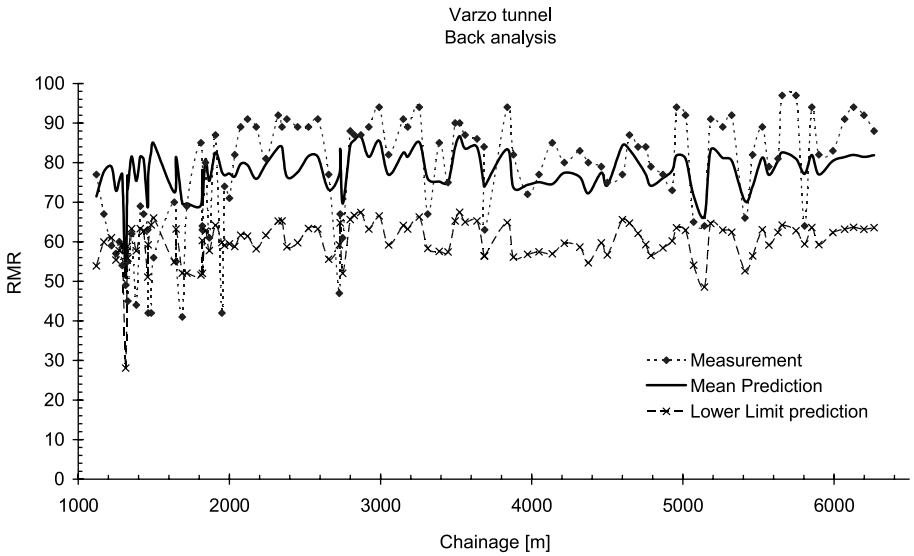

Fig. 17. Comparison of the estimated from field mapping and predicted RMR along the chainage of the Varzo tunnel by using the calibrated hyperbolic relationship

overburden is mostly in the range 200–300 m, decreasing to 100 m only where the tunnel underpasses a few deep transversal gullies. Except for a short terminal part in morainic soil, which was excavated with conventional methods, the tunnel runs through the Antigorio gneiss formations, belonging to the Pennidic Units of the Alpine range. The only rock formation is an orthogneiss composed of quartz, feldspar and mica; mica content (mostly biotite) is in the 10–20% range. Also in this case the SE values along the chainage of the tunnel were predicted and then the a, b constants were calibrated from least-square analysis of SE and available RMR values based on the proposed fractional relation. In this case as it is displayed in Fig. 17 the mean and lower 95% prediction limit of RMR values are given by the following equations

$$RMR_{\text{mean}} = 100 - \frac{1916}{SE + 5.1}, \qquad RMR_{\text{min}} = 77 - \frac{1217}{SE - 9} \tag{23}$$

wherein as above SE is expressed in MPa.

The fourth considered case is that of Maen tunnel located also in Northwestern Alps and presented in the paper of Sapigni et al. (2002). The rock units consist of metaophiolites, (serpentinite, metagabbro, metabasite, chlorite schist, talc schist) and meta-sediments (calc schist and silicate marble) belonging to the Zermatt-Saas Zone of the Pennidic Domain. The parent rocks were carbonate pelagic sequences and mafic crystalline rocks that underwent high-pressure low-emperature metamorphism during the early phases of the Alpine orogenesis. Schists and serpentinite show a foliated texture while metagabbro and metabasite are generally weakly foliated. The attitude of rock units is more or less uniform throughout the tunnel, at N220–270° E/35–45° (dip direction/dip), so that the longitudinal axis of the inclined tunnel (plunging direction N128° E) is almost normal to the schistosity. A major shear zone, 20 m in thickness, is encountered within the tunnel. It is composed of massive blocks of serpentinite and metagabbro of volume 0.5–1.5 m^3 embedded in a sheared matrix of talc and chlorite schists associated with cataclastic bands. Even if the fault zone was clearly recognized by the geological investigations, as soon as the excavation reached the adverse stretch, massive blocks jammed the TBM cutterhead. In the attempt to move back the TBM, a large face and roof collapse occurred involving an estimated volume of 150–200 m^3 of loosened rocks. The accident caused 4 months delay over the 14 months total construction time and it required an extensive grouting of the failed mass to be undertaken. Dataset for performance analysis consists of 330 records featuring TBM parameters (head thrust, net boring time, total boring time) and rock mass classification indices (RMR and Q). The open-type TBM allowed continuous surveying of the rock mass all over the tunnel length. RMR and Q were independently logged by surveying adjacent tunnel sections 5 m in length; penetration rate and advance rate were computed dividing the length of the surveyed section (5 m) by the net boring time and the total boring time, respectively.

Since for this tunnel both RMR and Q estimations were made the first thing was to put these data in a graph and then by using the logarithmic formula (19) to predict RMR from Q raw data. This comparison that gives additional validity to (19) is illustrated in Fig. 18. In this case the values of the a and b parameters of the hyperbolic

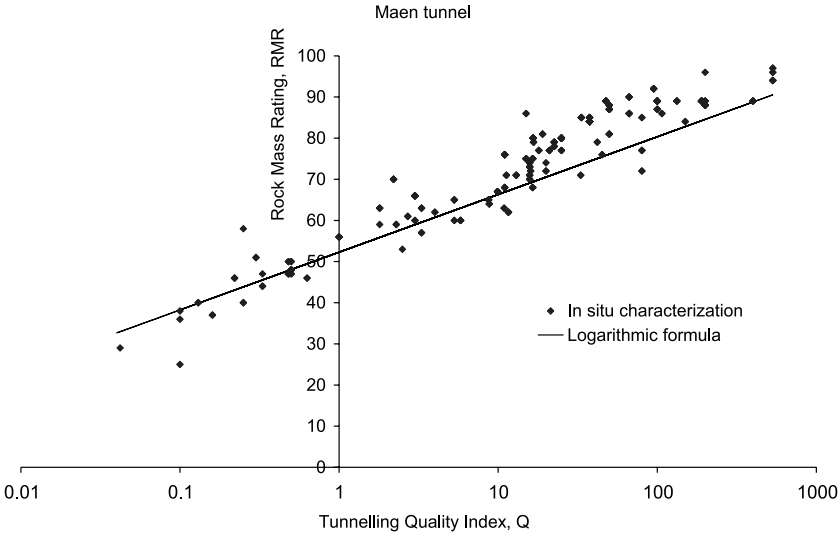

Fig. 18. Comparison of the raw data pertaining to RMR and Q estimations along the tunnel with the predictions of formula (19)

model linking RMR with SE were simply taken from the previously analyzed Varzo tunnel, i.e. $a = 1916$ MPa and $b = 5.1$ MPa. The good comparability of the predicted values of RMR with those actually inferred from the geotechnical mapping is displayed in Fig. 19.

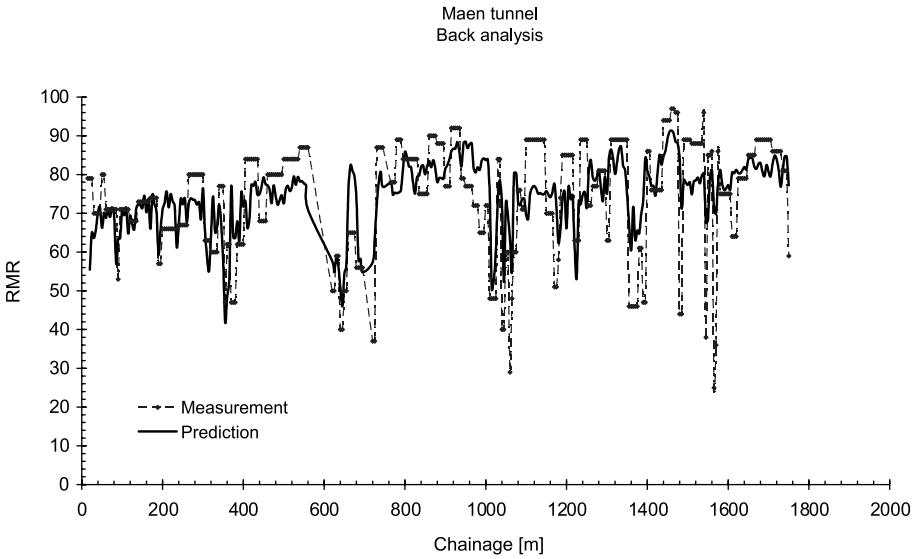

Fig. 19. Comparison of the measured and predicted RMR along the chainage of the Maen tunnel by using the calibrated hyperbolic relationship found from the Varzo tunnel

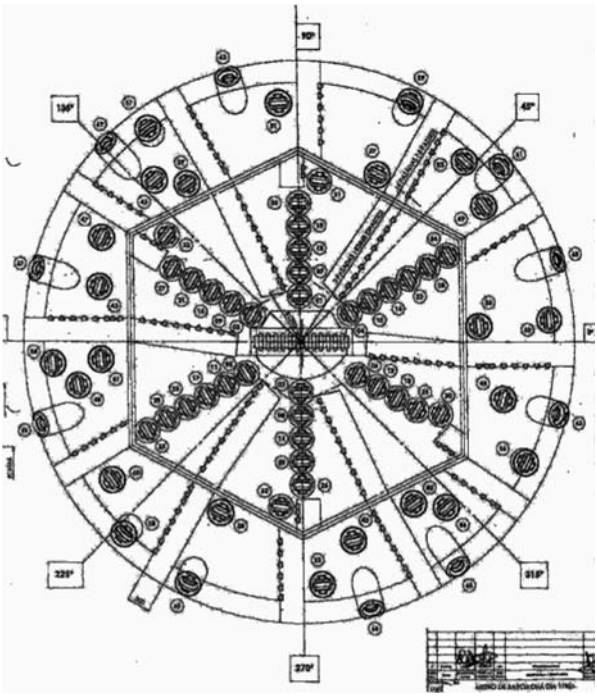

Fig. 20. Cutterhead of the NFM machine

3.3 L9 Barcelona Metro tunnel case study (Singuerlin-Esglesias section)

The last case study considered in this work is the Line 9 of Barcelona Metro that will interconnect with each of the existing metro lines, the suburban railway lines and with the high speed railway at 12 high-capacity interchange stations. In addition the line will connect the airport to the City, the Barcelona Fair, the courts district and pass under one of the main university campuses.

For the sections to be driven predominantly in hard rock (granodiorite, slates and cornubianites) a shielded NFM dual EPB/open type has been selected (Fig. 20). The machine is adaptable to work in closed mode if it is boring in unstable ground or fault zones. The main characteristics of the NFM machine are shown in Table 4.

The Barcelona area is composed of a Paleozoic crystalline basement of sedimentary origin including slates, limestone and micro-conglomerates which underwent a light regional metamorphism and cornubianites which were affected by a batholitic intrusion showing a certain degree of thermal metamorphism. These rocks, especially the granodiorite forming the batholith, show a high degree of weathering close to the surface. Lying on this Paleozoic basement is a Cenozoic series of Pliocenic argillites and Miocenic conglomerates (breccia type) with varying clay content. Further on top there exists a Quaternary series of alluvial and delta origin composed of clay, silts, sands and gravel, which are related to the fluvial bed of Llobregat y Besós rivers. Geological cross and plan-sections, borehole logs, laboratory data and TBM logs for *Singuerlin-Esglesias* section were collected and stored in a database.

Table 4. Characteristics of the NFM machine

Excavation diameter [m]	11.95
Total thrust [kN]	90,000
Articulation	11 cylinders × 350 mm
Head rotation speed [rpm]	0÷3.7
Max nominal torque [kNm]	27,000 at 1.25 rpm
Max breakout torque [kNm]	17,750
Max speed advance [cm/min]	8 (using all thrust cylinders)
Type	mixed shield: open or closed mode (EPB, air) permanently installed in the shield
Cutterhead	8 arms
Cutter tools	282 drag teeth, 69 disc cutters 17″ and 12 disc cutters 14″
Power	electrically powered, variable speed with vector flow control
Containment	compressed air or earth pressure, 3 bar maximum
Evacuation of spoil	screw conveyor or retractable extraction conveyor, two belt conveyors
Erector	6 degrees of freedom, rotation ± 220° semi-automatic erection of lining segments
Trailing train	6 trailers
Ancillary equipment	grouting injection system, proble drilling machine, injection of bentonite foam and mud

The geomorphology of the surface is rather smooth and there are not mentioned any karstic caves. The tunnel is below the water table.

No major faults are transecting the rock formations as it also appears in Fig. 21 that displays the conceptual geological longitudinal profile of that section. Also according to the plan-section of the area this profile remains more or less constant between the cross-sections. The geology of the area between Esglesia and Singuerlin tunnel stations consists of five individual geological formations. From the oldest -and deepest- to the newest, these are the following:

1. *Hard granodiorite rock (GR1)* slightly decomposed rock (grades I–III). This lithology covers the whole area. This layer is reached in depths from around 12–35 m from the surface. The TBM goes mainly through this hard granodiorite rock. That is the reason why in this area the open TBM mode is employed. The age of this layer is Palaeozoic.
2. *Fair Granodiorite (GR2)* highly decomposed (grades IV–V). This layer is reached in depths from around 0–16 m from the surface. This lithology also covers the whole area and for about 12 m we can see it in the surface, as well. The piezometric surface goes through this layer and also the layer below (*hard granodiorite rock*). The age of this layer is Palaeozoic.
3. *Clays with gravels and alluvium deposits (QCS)*. It is a layer of soft soil with gravel and alluvium deposits that covers the whole area between Esglesia and Singuerlin sections. This bed is found in depths of around 1–2 m and is practically the upper geological layer. Its age is Kenozoic.
4. *Debris (R)*. The depth of this layer is no more than 2 m.
5. *Magmatic Interventions (PF1) of Porfyrite*. They are slightly decomposed intrusions and the tunnel goes through them near the station of Singuerlin. There are 3 intrusions and the first to come across is in depth of 20 m. The other 2 are near the surface and their depth can be as much as 60 m. The thickness of these interventions ranges from some meters up to 20 m. The geotechnical properties are similar to the hard granodiorite rock. The age is Palaeozoic.

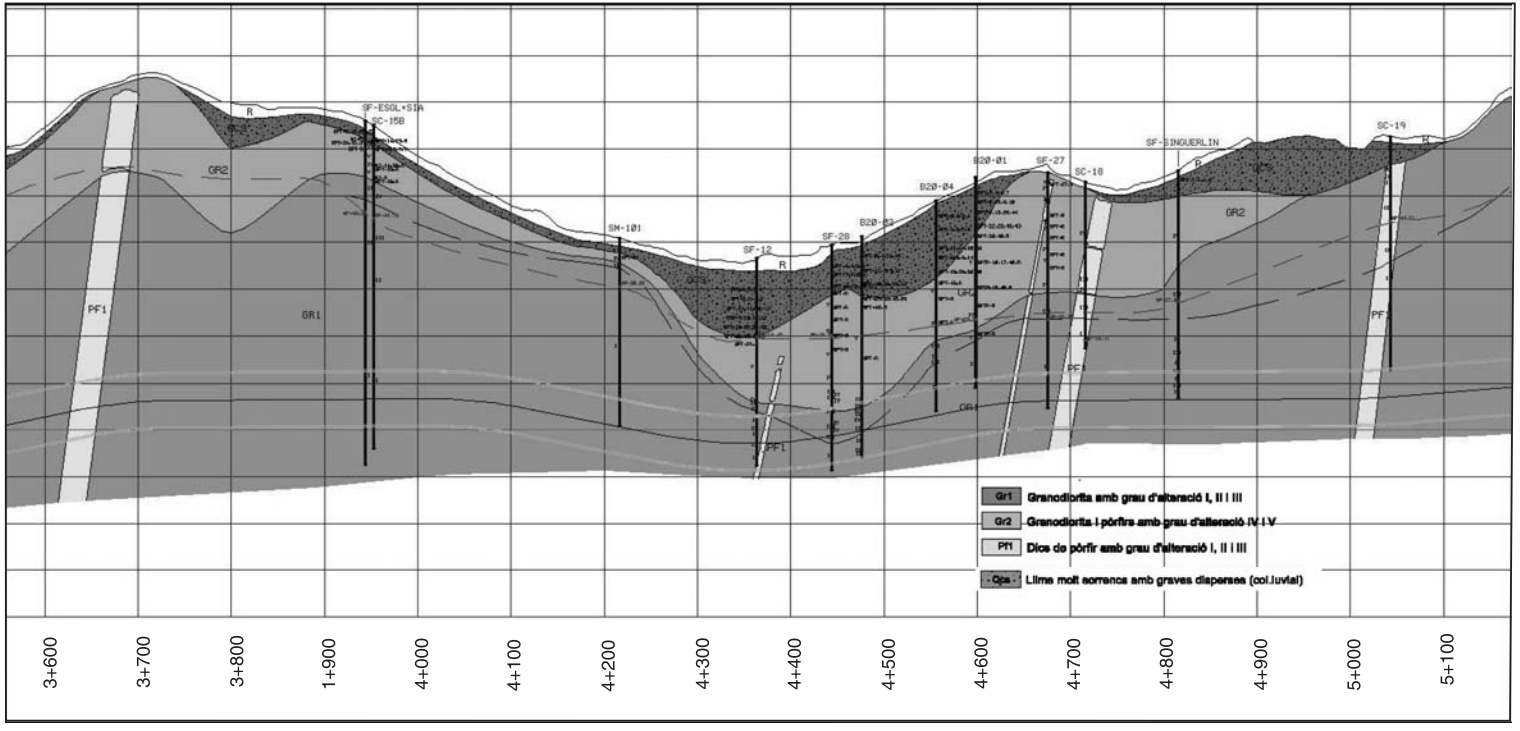

Fig. 21. Main geological profile of the Singuerlin-Esglesias section (L9 Barcelona)

In this project there are available only limited RMR logs and other geotechnical and lab data from cores collected along the boreholes as is indicated in Fig. 21. However, there are plenty TBM logs collected during rock excavation with the Wirth TBM machine. This set of data were collected during the excavation with a high frequency per concrete ring that was not appropriate for the purposes of this analysis and moreover was located at separate files. Therefore, in a first stage of analysis all the files were merged into only one Excel spreadsheet and the data were reduced so that a single row of logged data to correspond to each concrete ring as it is shown in Fig. 22.

From Fig. 23 it may be observed that for this case the T/F ratio does not follow closely the square root of penetration depth per revolution dependence except

Ring_number	tbmc	pushing	torque	ch_speed	ch_power	tbm_speed	penetration	mode	Thrust
	m	F (tn)	kN m	rpm	%	mm/min	mm/rev		kN
513	4700.00	2406.46	3723.25	3.67		17.09	4.66	N/A	24064.65
514	4698.04	2447.87	2536.74	3.67		11.29	3.07	Open	24478.7
515	4696.08	2424.21	1908.16	3.70	15	8.17	2.21	Open	24242.12
516	4694.12	2523.44	2889.72	3.66	17	12.66	3.45	Open	25234.41
517	4692.16	2542.87	3844.48	3.54	23	17.23	4.87	Open	25428.74
518	4690.20	2545.10	2987.36	3.71	24	13.52	3.64	Open	25451.02
519	4688.24	2453.45	3358.54	3.72	26	15.15	4.07	Open	24534.45
520	4686.28	2408.40	3775.51	3.68	26	17.93	4.87	Open	24084
521	4684.32	2415.20	3799.96	3.66	38	15.26	4.17	Open	24151.96
522	4682.36	2410.00	4417.98	3.66	23	18.06	4.94	Open	24100
523	4680.40	2440.17	4767.61	3.62		19.89	5.50	Open	24401.74
524	4678.44	2551.31	4457.98	3.69		18.63	5.05	Open	25513.05
525	4676.48	2577.71	2573.19	3.71	23	10.29	2.78	Open	25777.07
526	4674.52	2477.66	3753.28	3.72	23	14.27	3.83	Open	24776.61

Fig. 22. Excel worksheets referring to TBM logged parameters

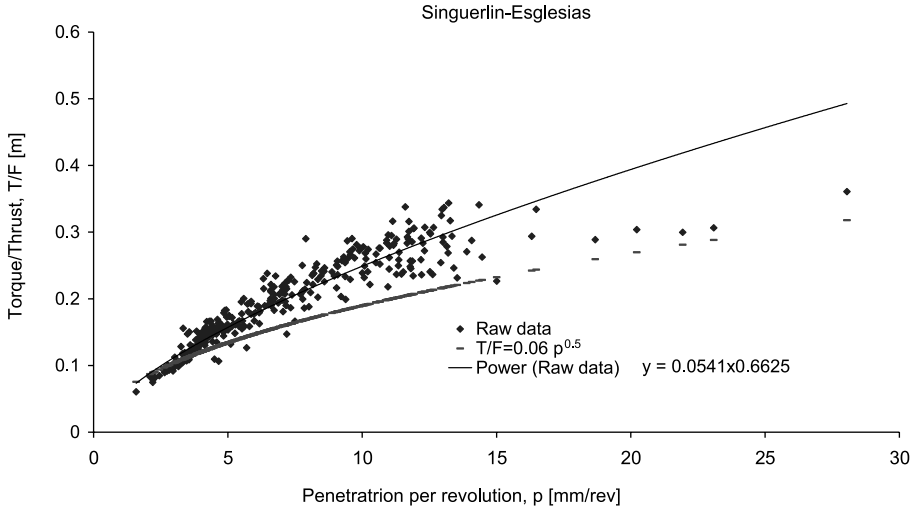

Fig. 23. Plot of the dependence of the T/F ratio on penetration depth per revolution

for lower T/F values and for large penetration depths. Instead the best-fitted power relation has the form

$$\frac{T}{F} = 0.0541 \cdot p^{0.6625} \tag{24}$$

where the ratio T/F has units of m and the penetration depth p of mm.

Based on the estimations of RMR from the available borehole logs, a 3D model of the spatial distribution of RMR was made by virtue of KRIGSTAT code. In this case the GR1, Pf1 and GR2 formations were independently modelled as 3D solids with an autodesk application, then they were discretized in the FLAC3D numerical code (Itasca, 2002) and the gridpoints of each formation where the Kriging estimations

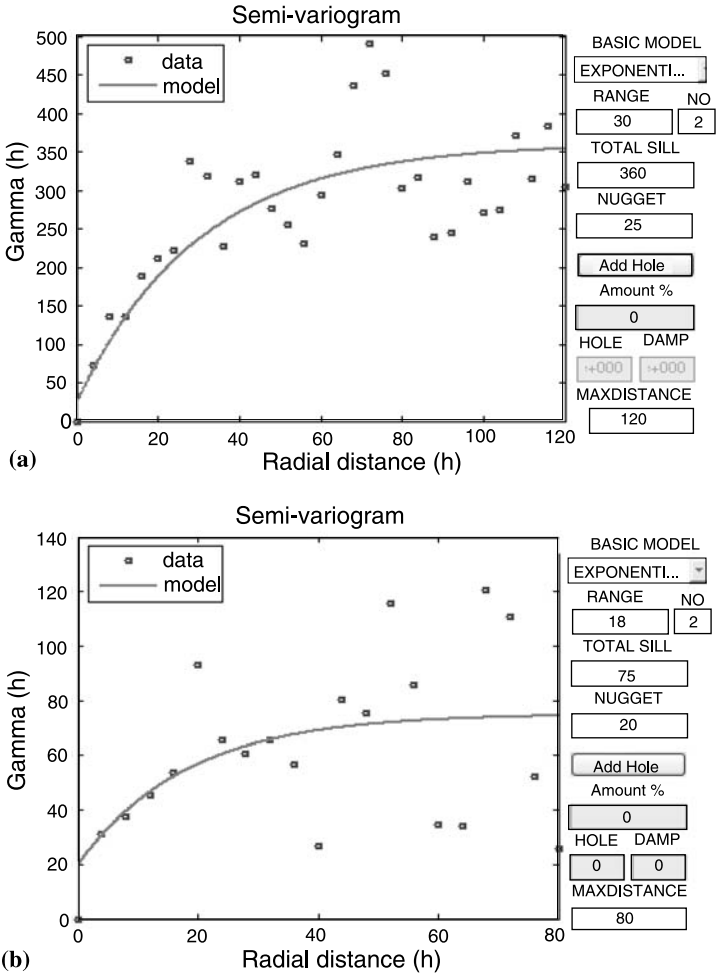

Fig. 24. RMR spatial distribution: (a) experimental and theoretical semivariogram model of the GR1 formation: exponential model, range = 30 m, sill = 360, nugget = 25, (b) GR2 formation: exponential model, range = 18 m, sill = 75, nugget = 20, (c) Kriging values and Kriging standard deviation (STD) estimations of the RMR distribution in the tunnel, and (d) in the complete volume model of both GR1, Pf1, and GR2 formations

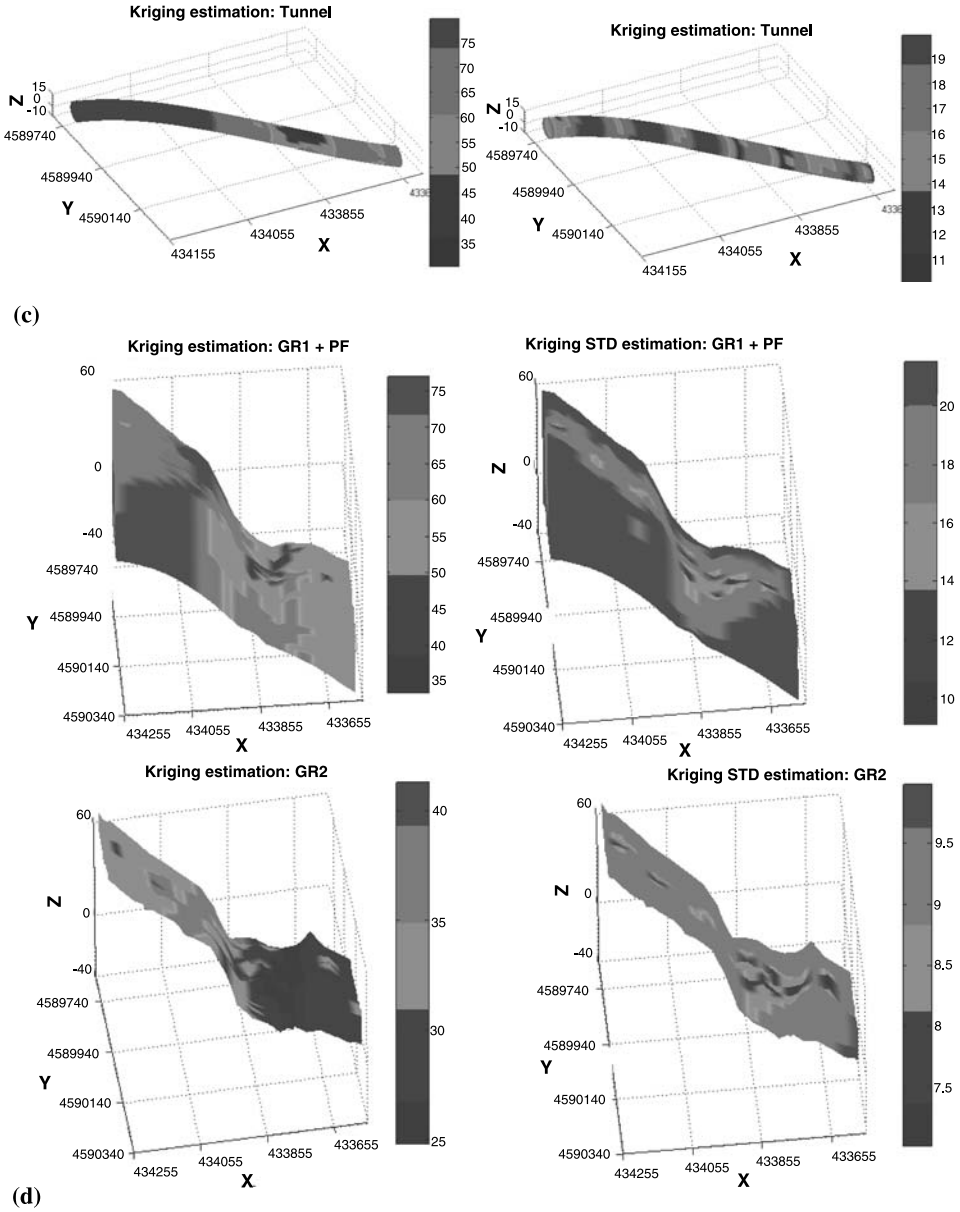

Fig. 24 (*continued*)

were performed were subsequently fed to KRIGSTAT code. The semivariograms for GR1 together with Pf1 (as a single volume model) and GR2 formations, respectively, created from the composited borehole (hard) data, by using a support of 2 m, are illustrated in Fig. 24a and b. Kriging estimations and errors based on these semivariograms are also displayed in Fig. 24c and d.

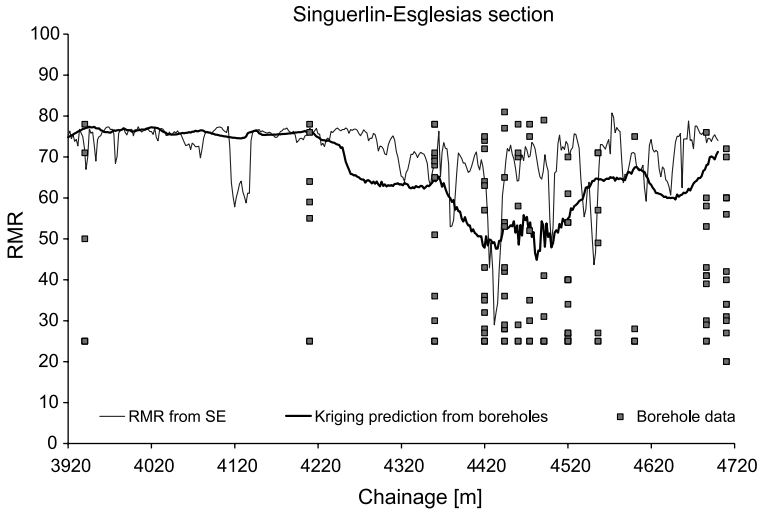

Fig. 25. Comparison of RMR prediction by the hyperbolic formula (20) and SE of TBM with the RMR evaluated from drill cores extracted from exploratory boreholes

As illustrated in Fig. 25 in which we have plotted the Kriging prediction of RMR distribution along the chainage, together with the RMR values sampled along the boreholes, the most important conclusion that can be drawn, is that if the SE estimations from TBM registered parameters are plugged-in the relationship (20) with initial estimations of a, b as given in the same relation, then the predicted RMR from the consumed SE of the TBM compare well with the max RMR inferred from the examination of the borehole cores. Hence, by taking also into account the inherent uncertainty of the borehole data and their variability due to smaller support of 2 m compared to TBM, the two parameters a and b of the hyperbolic relationship do not need further tuning.

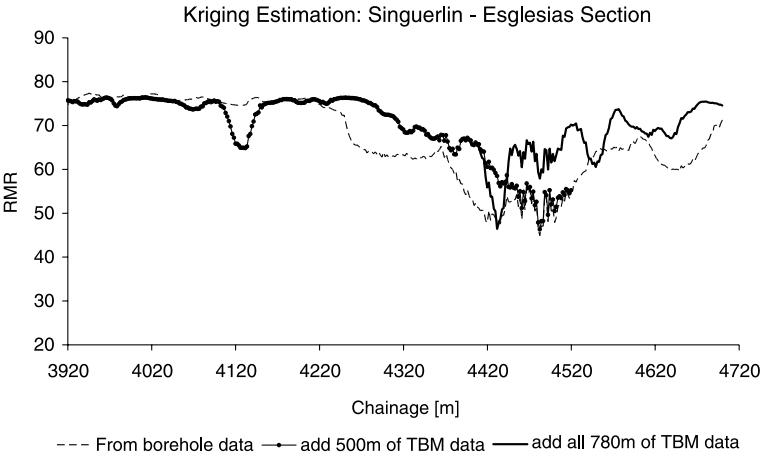

Fig. 26. Upgrade of the initial RMR Kriging model with TBM SE data up to the first 500 m and 780 m of tunnel advance, and prediction for the next 100 m ahead of tunnel's face for each of the two cases

The RMR estimations along the tunnel from the TBM data by virtue of relationship (20) during TBM advance are combined with the borehole data in order to upgrade the initial geotechnical model (RMR model) derived from the Kriging analysis of borehole data (i.e. that shown in Fig. 24a–d). This procedure of gradual upgrading of the semivariogram and the Kriging model was done for every 100 m of TBM advance with the prediction of RMR at 100 m ahead of the face of tunnel. This procedure is graphically for two cases is shown in Fig. 26.

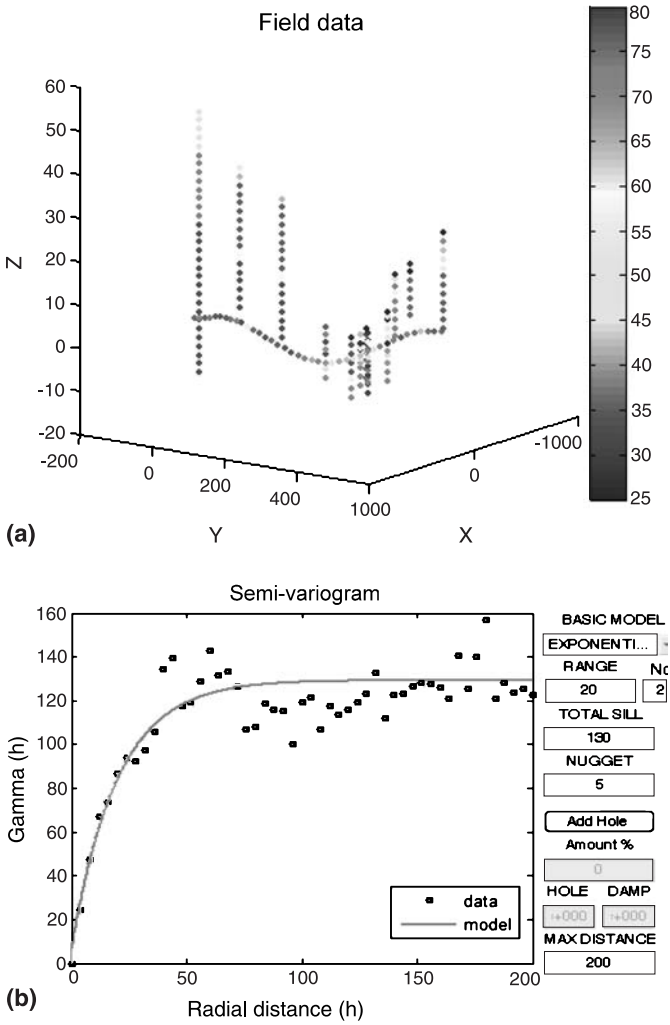

Fig. 27. Final RMR Kriging model created from all TBM SE data along the tunnel (colour bars indicated RMR values): (a) visual representation of RMR field data coming from boreholes and the tunnel, (b) experimental and theoretical semivariogram of the final model, (c) spatial distribution of RMR and of the Kriging error (STD) in the tunnel, and (d) distribution of RMR and the Kriging error of estimation in the whole model of GR1 and Pf1 formations

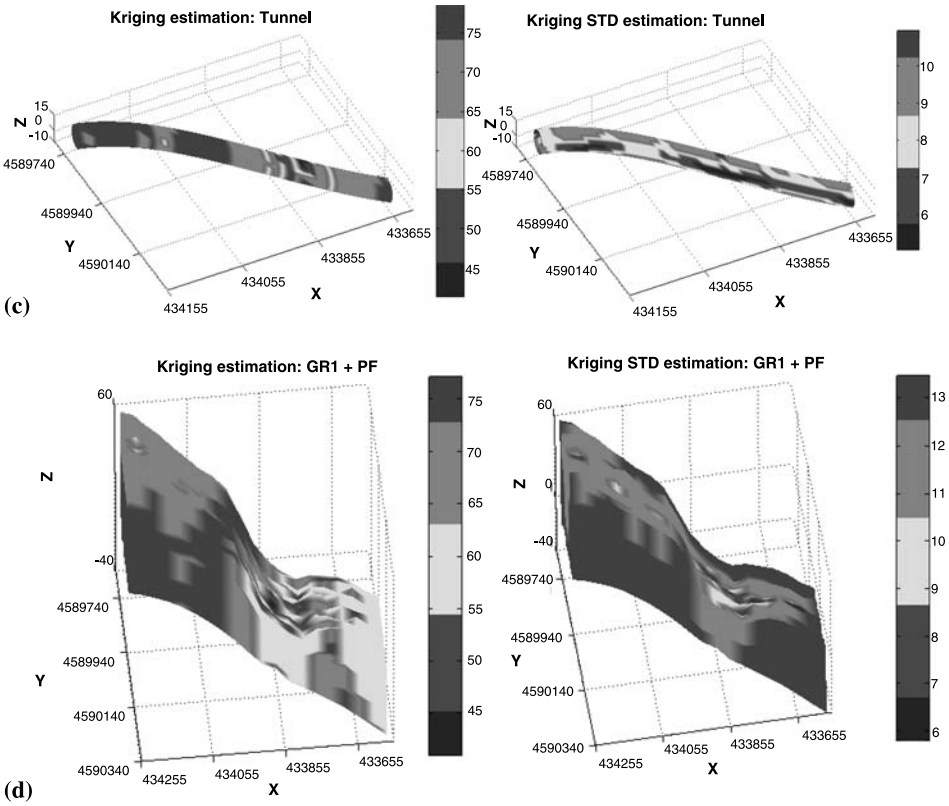

Fig. 27 (*continued*)

As a final result of the proposed method of analysis, we present in Fig. 27 the final model predictions by considering in the Kriging model in combination with the sampled data from boreholes also the estimated RMR data from the analysis of the TBM logged data along the entire length of the tunnel. It may be noticed that the updated semivariogram of GR1 is similar to that estimated from the boreholes (e.g. Fig. 24a) but it is characterized by a lower sill due to decrease of the variance of the statistical distribution, and that the Kriging error of estimation along the tunnel and in the GR1 model estimated with the upgraded model (Fig. 27c and d, respectively) is lower always than that found by using the boreholes only (e.g. Fig. 24c and d).

4. Concluding remarks

A central problem of major practical significance in rock excavation engineering is the prediction of spatial distribution of rock strength (and possibly abrasivity parameters such as Cerchar or LCPC) over the tunnel length by using the limited number of samples from boreholes. If such a methodology is found, then the most probable values for penetration rate and wear of a TBM would be predicted and the rock mass mechanical behaviour due to excavation would be also inferred before the commencement of excavation.

Herein a first attempt is performed to attack the above problem by virtue of an algorithm that it is based on the following steps:

(a) Estimation of rock mass classification indices such as RMR or Q from borehole data (if such data are available).
(b) The creation with an autodesk application of the 3D volume geological model comprised from the various distinct geological formations.
(c) Discretization into finite elements of each of these solid models of rock formations, separately.
(d) Calculation of the SE consumed by the TBM by means of simple analytical relations.
(e) Use a simple hyperbolic function linking SE with rock mass classification index (i.e. RMR or Q) with only two calibrating constants. These constants may be calibrated based on the SE data collected during a certain distance traveled by the TBM inside a characterized rock formation either from boreholes or from surface mapping inside the tunnel (e.g. Fig. 1).
(f) Upgrading of the first 3D Kriging model derived only from borehole data by using also available TBM data to predict RMR or SE ahead of the tunnel's face (e.g. Figs. 26 and 27).

The Kriging technique is used here for the interpolation of rock mass classification data, as well as TBM data between arbitrary sampling locations in each geological formation separately, by employing the tool of the semivariogram (i.e. the mean square two-point difference of measurements). The arguments in favor for using the Kriging technique are the following: first of all the fact that geological materials are heterogeneous and their properties (strength, abrasivity, joint frequency, etc) may display a spatial structure or spatial correlation (i.e. in that case they are not purely random processes such as a Poisson process); also this technique apart from its simplicity gives the Best Linear Unbiased Estimations (BLUE) at any location between sampling points; furthermore unlike other estimation procedures, Kriging provides a measure of the error or uncertainty of the estimation, and finally it may be employed to find the spatial distribution of rock strength and abrasivity parameters (e.g. Cerchar or LCPC) over the tunnel length by using limited number of samples coming from exploratory boreholes, in order to predict in a next phase the most probable values for penetration rate and wear.

The main conclusions drawn from this preliminary study are the following:

(i) the inverse dependence of RMR on SE with a simple hyperbolic expression, and the relatively good applicability of this analytical relationship in all the considered tunnel cases in this study,
(ii) it was also confirmed in this study that RMR is linked with Q via a logarithmic relation,
(iii) the good agreement of RMR predictions from the borehole Kriging model with the RMR prediction estimated from the SE of TBM in the L9 case study, and
(iv) the demonstrated possibility of application of a gradual upgrading Kriging procedure for the prediction of RMR along the tunnel based on SE estimations in the L9 tunnel section.

Appendix A

The updated flowchart of KRIGSTAT code written in Fortran 77 is presented in Fig. A.1. All the subroutines of the code were compiled at the Matlab (2000) environment in order to generate executable files of the *.dll* format. With this scheme we combine the advantages of using the graphics tools of Matlab and the computational capabilities and speed of FORTRAN. The Kriging code consists from five separate parts from A to E. Part A is a pre-processor performing classical statistical analysis of the data. Part B refers to the construction of the experimental semivariogram and the best-fitting of the theoretical semivariogram function for the subsequent spatial data analysis. Part C performs the validation of the selected theoretical semivariogram function. Part D refers to the creation of the Kriging model of the spatial variable at hand. Finally, Part E is the post-processor for visualization and processing of the

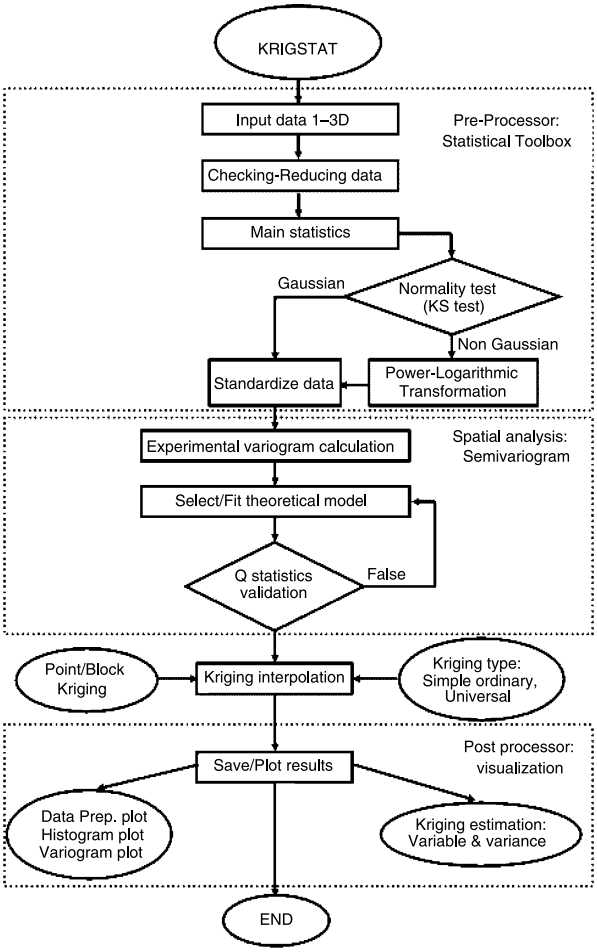

Fig. A1. Flowchart of the upgraded Kriging interpolation code KRIGSTAT

Table A.1. Description of the subroutines and functions performed by them in the upgraded KRIGSTAT code

Part/action		Name of subroutine	Input		Output	
A.1. Correction of data		CORRECT	X, Y, Z V ytox, ztox UL, LL	coordinates value units transformation upper & lower limit	Vc Xc, Yc, Zc	value coordinates
A.2.1. Compositing of drillhole samples		DRILLHOLE	DAT ID X, Y, Z L1, L2 V leng	Id number of drillhole coordinates start – end length value length	Vb IDb Xb, Yb, Zb	value Id number of drillhole coordinates
A.2.2. Reduce/ Smoothening/ grouping of data	radial mask	RANDCOMP	X, Y, Z, V D R FLT	 grid distance search radius Filter 1 nearest 2 mean 3 median	Vr	value
	block mask	BLCOMP	X, Y, Z, V DX, DY, DZ FLT	 sizes of block		
	reduce mask	REDDAT	X, Y, Z, V V NR SP FLT	 value reduction factor support number	Xr, Yr, Zr	coordinates
A.3.1. Compute main statistics and normality test (KS)		STAT	V	value	mean, SV, median, Skewn, STD, Kurt save file = 'STATISTICS.TXT'	
A.3.2. Kolmogorov-Smirnov test		KST	V CL	value confidence level: 1, 2, 5, 10, 20	D Dcl pval	KS statistic limit on CL probability
A.4. Cox-Box transformation		TRANSVAL	V type Is c1, c2, c3, base	value 1 logarithmic 2 power 1 direct 2 inverse 1. $Z = c1 \log (c2\,V + c3)/\log (base)$ 2. $Z = c1\,(V^{base}\text{-}c3)/c2$	Z	transformed value
A.5. Standardize data		NORMALIZE	X, Y, Z, V STD, mean M1	 0 skip 1 axis trans to min (X, Y, Z) 2 isotropic 3 standard cube (a = 1) for coordinates	Vout	value

(*continued*)

Table A.1 (*continued*)

Part/action	Name of subroutine	Input		Output	
		M2	0 skip 1 to mean = 0 2 to STD = 1 3 to mean = 0 & STD = 1 for value	Xout, Yout, Zout	coordinates
B. Compute experimental semivariogram	SEMIVAR	variance X, Y, Z, V lag distances PHI, THETA Rtol DPHI, DTHETA BWH, BWD OPT	 directions of search distance tolerance angle tolerances bandwidths, horizontal and vertical 'ORIGINAL' OR 'TRANS' due to anisotropy correction	no gamma Vg	number of pairs semi- variogram variance of estimation gamma
C.1. Q validation test	QVAL	CX V the rest of the input variables are given below in BLKRIG3D (from range to infinity)	[X, Y, Z] variable	Q1 L1 U1 Q2 L2 U2	Q1 statistic lower limit upper limit Q2 statistic lower limit upper limit
C.2. Leave one out cross-validation test	LEAVE1OUT			DATout Vout Svout	[X, Y, Z] estimation square error estimation
D. Kriging interpolation	BLKKRIG3D	CX V CXO R Phi model Sill He D CH DC RC BLK ND MBT MG IS IT	[X, Y, Z] variable [Xo, Yo, Zo] estimation points range (−s) anisotropy angles theoretical semivariogram types: 1) Nugget, 2) exponential, 3) Gaussian, 4) spherical, 5) piecewise linear, 6) quadratic, 7) cubic, 8) linear, 9) hole effect Sill of semivariogram hole effect damping parameter starting lag of semivariogram maximum lag relative range block size discretization of block 1 for point 2 for block Kriging 1 for variogram 2 covariance 0 anisotropic, 1 isotropic 1 simple 2 ordinary 3 universal	DATout Vout Svout	[X, Y, Z] estimation square error estimation

(*continued*)

Table A.1 (*continued*)

Part/action	Name of subroutine	Input		Output
		SCUT	square error estimation upper limit	
		AVG	global mean	
		SR	radius of neighbourhood	
		MNXPTS	minimum used points	
		MXPTS	maximum used points	
		eps	a very small value	
		INF	infinity	
E. Post processor	visualization and validation of predictions			

quanitative data. As the flowchart of Fig. A.1 and Table A.1 indicate, the steps involved in the Geostatistical Analysis are the following:

1. Checking and compositing of sampled data (Part A).
2. Computation of the raw data statistical distribution and its parameters (mean value, variance, skeweness, kyrtosis, etc.) (Part A).
3. Checking for outliers (Part A).
4. Checking for necessity of nonlinear transformation of data (due to asymmetry, heavy tails) (Part A).
5. Computation of the experimental semivariogram (Part B).
6. Sensitivity analysis for the semivariogram parameters such as lag, tolerance, range, etc. (Part B).
7. Check for possible anisotropy (direction of searching, tolerance, etc.) (Part B).
8. Check for trend of data (Part B).
9. Selection of the theoretical model and best-fit of theoretical semivariogram (Part B).
10. Validation of the semivariogram model (Part C).
11. Selection of the Kriging model (i.e. ordinary, universal, block, etc.) and its parameters such as the max Kriging radius, minimum and maximum Kriging points (Part D).
12. Prediction of the variable of interest and the Kriging variance (error) at selected nodes in the domain (Part D).
13. Validation of Kriging predictions and visualization of raw data and model predictions (Part E).

Acknowledgements

The authors would like to sincerely thank the financial support from the EC 6th Framework Project TUNCONSTRUCT (Technology Innovation in Underground Construction) with Contract Number: NMP2-CT-2005-011817.

References

Barton N (2000) TBM tunnelling in jointed and faulted rock. Balkema, Rotterdam

Barton N, Lien R, Lunde J (1974) Engineering classification of rock masses for the design of rock support. Rock Mech 6: 189–236

Bieniawski ZT (1973) Engineering classification of jointed rock masses. Trans S African Instn Civ Engrs 15(12): 335–344

Fukui K, Okubo S (2006) Some attempts for estimating rock strength and rock mass classification from cutting force and investigation of optimum operation, of tunnel boring machines. Rock Mech Rock Engng 39(1): 25–44

Gertsch R, Gertsch L, Rostami J (2007) Disc cutting tests in Colorado Red Granite: implications for TBM performance prediction. Int J Rock Mech Min Sci 44: 238–246

Itasca Consulting Group Inc. (2002) FLAC3D, Fast Lagrangian Analysis of Continua in 3 Dimensions: User's Guide. Minneapolis, Minnesota USA

Journel AG, Huijbregts CHJ (1978) Mining geostatistics. Academic Press, London

Kitanidis PK (1997) Introduction to Geostatistics: Applications in Hydrogeology, Cambridge University Press, United Kingdom

Kutter HK, Sanio H-P (1983) Discussion of paper by Snowdon RA, Ryley MD and Temporal J, ''A study of disc cutting in selected British rocks''. Int J Rock Mech Min Sci Geomech Abstr 19: 107–121: (1982) Int J Rock Mech Min Sci Geomech Abstr 20(2): 103–104

Matlab 6.0 (2000) The Mathworks Inc., Natick, Massachusetts, USA

Papoulis A (1984) Probability, random variables and stochastic processes. McGraw-Hill International Editions, Singapore, 576 pp

Ribacchi R, Lembo Fazio A (2005) Influence of rock mass parameters on the performance of a TBM in a gneissic formation (Varzo Tunnel). Rock Mech. Rock Engng 38(2): 105–127

Rostami J, Ozdemir L (1993) A New Model for Performance Prediction of Hard Rock TBMS. Chapter 3 in 1993 RETC PROCEEDINGS, 793–809

Roxborough FF, Phillips HR (1975) Rock excavation by disc cutter. Int J Rock Mech Min Sci Geomech Abstr 12: 361–366

Sapigni M, Berti M, Bethaz E, Busillo A, Cardone G (2002) TBM performance estimation using rock mass classifications. Int J Rock Mech Min Sci 39: 771–788

Stavropoulou M, Exadaktylos G, Saratsis G (2007) A combined three-dimensional geological-geostatistical-numerical model of underground excavations in rock. Rock Mech Rock Engng 40(3): 213–243